Biomech Model Mechanobiol (2016) 15:133–154
DOI 10.1007/s10237-015-0707-8

ORIGINAL PAPER

Molecular and intermolecular effects in collagen fibril mechanics: a multiscale analytical model compared with atomistic and experimental studies

Michele Marino[1]

Received: 30 January 2015 / Accepted: 13 July 2015 / Published online: 30 July 2015

Abstract Both atomistic and experimental studies reveal the dependence of collagen fibril mechanics on biochemical and biophysical features such as, for instance, cross-link density, water content and protein sequence. In order to move toward a multiscale structural description of biological tissues, a novel analytical model for collagen fibril mechanics is herein presented. The model is based on a multiscale approach that incorporates and couples: thermal fluctuations in collagen molecules; the uncoiling of collagen triple helix; the stretching of molecular backbone; the straightening of the telopeptide in which covalent cross-links form; slip-pulse mechanisms due to the rupture of intermolecular weak bonds; molecular interstrand delamination due to the rupture of intramolecular weak bonds; the rupture of covalent bonds within molecular strands. The effectiveness of the proposed approach is verified by comparison with available atomistic results and experimental data, highlighting the importance of cross-link density in tuning collagen fibril mechanics. The typical three-region shape and hysteresis behavior of fibril constitutive response, as well as the transition from a yielding-like to a brittle-like behavior, are recovered with a special insight on the underlying nanoscale mechanisms. The model is based on parameters with a clear biophysical and biochemical meaning, resulting in a promising tool for analyzing the effect of pathological or pharmacological-induced histochemical alterations on the functional mechanical response of collagenous tissues.

✉ Michele Marino
marino@ikm.uni-hannover.de

[1] Institute of Continuum Mechanics, Leibniz Universität Hannover, Appelstraße 11, 30167 Hannover, Germany

Keywords Mechanics of collagen fibrils · Cross-link density · Elasto-damage response · Hysteresis behavior · Multiscale modeling

1 Introduction

Collagen is an ubiquitous protein, representing the main constituent of connective tissues in vertebrates. It can be found in more than 27 forms, but type I collagen is the most abundant in the human body, being the most important for maintaining the structural integrity and a functional mechanical behavior of structural tissues, such as cartilage, bones, tendons, ligaments, and vessel walls, (Fratzl 2008).

Type I collagen molecule is made up by three polypeptide strands which form a triple-helix quaternary structure, stabilized by interstrand hydrogen weak bonds. These molecules exhibit hydroxyproline-deficient sequences characterized by 60 residues (about 20 nm long), referred to as labile domains or molecular kinks (Miles and Bailey 2001; Fratzl 2008). Molecular kinks are activated by thermal fluctuations (Misof et al. 1997) and can be extended by forces at molecular ends that counteract thermal undulations. This mechanism is related to the flexural behavior of macromolecular segments and is known as entropic elasticity (Marko and Siggia 1995; Buehler and Wong 2007; Fratzl 2008). It couples with elastic mechanisms associated with the uncoiling of collagen triple helix and the stretching of molecular backbone, known as energetic elasticity (Buehler 2006; Holzapfel and Ogden 2010; Maceri et al. 2012b; Marino and Vairo 2013).

Collagen molecules assemble themselves in ordered and staggered arrays (Holmes et al. 2001). The latter are, in turn, arranged to form a supertwisted and discontinuous right-handed microfibril which interdigitates with neighboring microfibrils and form thin (20–500 nm) and long (>1 mm)

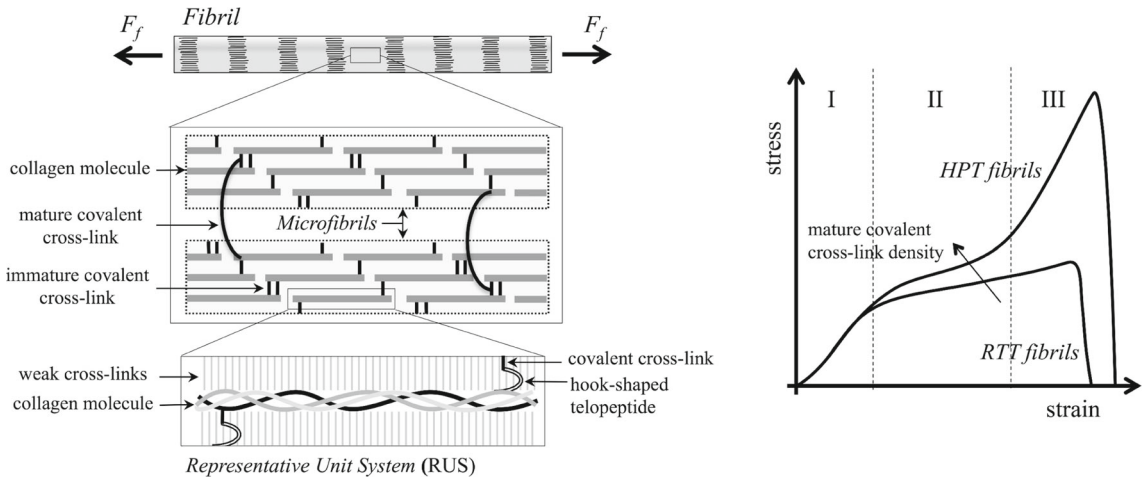

Fig. 1 *Left* Fibril multiscale structure. The hierarchical organization of triple-helix collagen polypeptides, cross-linked by immature and mature enzymatic cross-links. Definition of the representative unit system (RUS). *Right* Typical stress–strain responses of collagen fibrils from human-patellar tendon (HPT) and rat-tail tendon (RTT) where a different density of mature covalent cross-links occurs. Three distinct regions (denoted as *I*, *II*, and *III*) are experimentally observed

fibrils at the mesoscale (nano-to-micro). Fibrils collect themselves in form of fibers at the scale of micrometers (Orgel et al. 2006; Fratzl 2008).

Aside from weak interactions among molecules, the fibrillar structure is stabilized by intermolecular covalent cross-links of which two main types have been identified (Eyre and Wu 2005; Avery and Bailey 2008). A first type results from advanced glycation end products (AGEs) whose sources, formation pathways and chemical structure are yet not fully characterized (Reiser et al. 1996; Bailey et al. 1998; Bailey 2001; Depalle et al. 2014). AGEs accumulate with age and diabetes and may impair fibrils normal function, being associated with pathological alterations in tendon stiffness and viscoelasticity (Andreassen et al. 1981; Li et al. 2013), in bone toughness and ductility (Zimmermann et al. 2011), in cartilage stiffness and fragility (Verzijl et al. 2002; DeGroot et al. 2004).

A second covalent cross-link type (namely, the enzymatic cross-link) is essential in the maturation and the physiological mechanical function of collagen fibrils (Brüel et al. 1998; Bailey 2001; Eyre and Wu 2005; Fessel et al. 2012; Svensson et al. 2013; Depalle et al. 2014). It is promoted by the enzyme lysyl oxidase acting on specific lysine amino acids of molecular non-helical ends (both at N- and C-terminal). The resulting allysine reacts with a specific lysine of an adjacent molecule, forming a divalent intermolecular bond (Bailey 2001; Eyre et al. 2008; Wess 2008). Using X-ray diffraction techniques, it has been shown that the C-terminal cross-link forms on a telopeptide that takes a folded hook-shaped configuration, adding nonlinearities to fibril mechanical behavior (Orgel et al. 2000; Wess 2008; Uzel and Buehler 2011; Marino and Vairo 2014a). These divalent bonds are referred to as immature. In fact, over time, these may further react with another telopeptide aldehyde group, forming a trivalent mature bond linking three collagen molecules (Bailey 2001; Avery and Bailey 2008; Eyre et al. 2008). Bailey et al. (1998) proposed that mature cross-links form between molecules on different microfibrils and fibrils (Avery and Bailey 2008).

In this study, enzymatic cross-links are focused only and Fig. 1 schematically shows the features of fibril hierarchically organized structure herein addressed. Significant variations in enzymatic mature cross-links concentrations have been reported in different tissues (Eyre et al. 1984; Saito et al. 1997). For instance, Saito et al. (1997) reports that the density of trivalent cross-links for middle-age men is 280 mmol/mol in skin, 390 mmol/mol in bone and 1800 mmol/mol in articular cartilage. On the other hand, the density of immature cross-links appears to be fairly constant across different tissues resulting 1340 mmol/mol in cartilage, 1350 mmol/mol in bone and 1590 mmol/mol in skin for middle-age men (Saito et al. 1997).

The load transmission within fibrils is highly affected by the presence or by the lack of mature cross-links because these cross-links between twisted microfibrils prevent intrafibrillar sliding mechanisms (Yang et al. 2012). Accordingly, the alteration in the biochemistry of these cross-links is an effective strategy for tuning the mechanical properties of tissues such as, for instance, their strength and stiffness (Carmo et al. 2002; Fratzl 2008; Fessel et al. 2012; Yang et al. 2012; Svensson et al. 2013). In general, fibrils subjected to a monotonic uniaxial traction present a stress–strain constitutive response characterized by three distinct regions: an initial rise in modulus (region I) followed by a plateau with reduced modulus (region II), which is finally followed by an even greater increase in stress and

modulus before failure (region III; Svensson et al. 2013). Nevertheless, different mature cross-link density has been associated with significant differences in fibril constitutive response: fibrils in adult human-patellar tendons (HPTs) are characterized by about 890 mmol/mol mature cross-links and display a well-rendered region III of increasing modulus at high strains before abrupt failure (Svensson et al. 2013). In contrast, the density of mature cross-links in fibrils of rat-tail tendons (RTTs) is very low (about 8.7 mmol/mol) and their constitutive response displays a plateau leading up to failure with region III being almost absent (Svensson et al. 2013). Because of these different curve shapes and as schematically shown in Fig. 1, human-patellar fibrils fail at significantly higher stress than rat-tail fibrils and appear more brittle.

Understanding the relationship between biochemistry and mechanics in collagen fibrils is an open topic which is nowadays widely investigated (Uzel and Buehler 2011; Svensson et al. 2013; Marino and Vairo 2014a; Depalle et al. 2014). In fact, it would open toward the better comprehension of: physiological functional behavior of tissues in living and remodeling organs; pathological tissue mechanical dysfunctions associated with histochemical alterations; self-healing processes or pharmacological treatments. To this aim, internal deformation and failure mechanisms have to be elucidated, and their effects on fibril behavior should be described and analyzed. A wide literature exists on this field by following both experimental studies (Sasaki and Odajima 1996; Saito et al. 1997; Orgel et al. 2000; Bozec and Horton 2005; Orgel et al. 2006; Svensson et al. 2013) and atomistic computational approaches (Buehler 2006; Buehler and Wong 2007; Buehler 2008; Uzel and Buehler 2011; Depalle et al. 2014). Both approaches are incomparable resources for clarifying the in vivo, in vitro and in silico mechanical behavior of collagen molecules, cross-linked molecular assemblies, and entire fibrils. Nevertheless, from both aforementioned approaches, some limitations arise due to the complexity of the systems under investigations and the wide differences in the involved length scales. In fact, experimental techniques reach their limits in distinguishing molecular and intermolecular effects occurring within fibrils. On the other hand, molecular dynamics simulations (MDSs) at the atomic scale are feasible in terms of computational costs only for short cross-linked assemblies (long only few hundreds of nanometers; Uzel and Buehler 2011; Gautieri et al. 2014) even employing coarse-grained molecular descriptions (Buehler 2008; Depalle et al. 2014). Moreover, atomistic modeling requires the use of large deformation rates that often lead to underestimate molecular entropic effects and to overestimate the forces computed during the simulations (Klepeis et al. 2009; Depalle et al. 2014). Finally, the high computational cost of MDS prevents from the development of extensive parametric simulation campaigns and makes these simulations unhelpful at the scale of tissues and organs.

In this paper, starting from well-established experimental and atomistic computational evidence, an analytical model of collagen fibrils is presented, opening to parametric and low computing-cost simulations with a detailed insight on the elasto-damage mechanisms at nanoscale. Reference is made to the fibril multiscale model proposed by Marino and Vairo (2014a), in the following referred to as the *MV-model*, which allows to analyze the general influence of intermolecular effects on fibril mechanics. The MV-model, based on an internal constrained variational framework, starts from the definition of a nanoscale representative unit system (RUS, see Fig. 1) for the fibril. The RUS describes the main mechanical features that have to be upscaled, and it is analogous to the representative volume element in homogenization approaches (Kouznetsova et al. 2001; Hain and Wriggers 2008; Lehmann et al. 2012; Marino and Vairo 2014b). The definition of interscale compatibility relationships and of constitutive responses for the nanoscale constituents allows to obtain fibril constitutive response, explicitly based on the actual histochemical environment through model parameters with a clear physical sense. Moreover, this analytical approach might be employed within a structural multiscale approach for developing refined microscale models of collagen fibers and macroscale models of biological tissues (Maceri et al. 2010, 2012a, 2013; Marino and Vairo 2013, 2014b, c), opening to simulations of entire organs.

Nevertheless, the MV-model does not account for molecular entropic/energetic nonlinearities, and model outcomes have not been compared with fibril experimental constitutive responses. Since the multiscale approach proposed by Marino and Vairo (2014a) can straightforwardly incorporate refinements in the description of nanoscale constituents, the MV-model is here enriched. Both weak and covalent intermolecular interactions are addressed and coupled with a refined molecular description involving both entropic and energetic elasticity (Maceri et al. 2012b). Damage mechanisms involving both collagen molecules and their interactions are taken into account. Accordingly, the role of density and maturation of enzymatic cross-links on fibril elasto-damage response are investigated by showing their influence on the dominant mechanisms determining fibril internal elasto-damage mechanisms and, thereby, on their overall response. Model outcomes are compared with available atomistic results (Buehler 2008) and experimental data (Svensson et al. 2013), proving model effectiveness in capturing fibril mechanical behavior at different cross-link-related biochemical conditions. Moreover, the typical hysteresis behavior of collagen fibrils is recovered.

2 Multiscale model

The model is developed within the context of standard generalized materials (Germain et al. 1983; Frémond 2002) and by

adopting a time-incremental operative framework. Accordingly, introducing the time variable τ and the time increment $d\tau$, the value of a given quantity x at the actual time $\tau = t$ is obtained by superimposing the perturbation $dx = \dot{x}d\tau$ to the reference value $\bar{x}$ relevant to the time $\bar{t} = t - d\tau$, where $\dot{x}$ is the left-hand time derivative of x at t, in agreement with the causality principle. Moreover, $(O, \boldsymbol{\xi}_1, \boldsymbol{\xi}_2, \boldsymbol{\xi}_3)$ is the three-dimensional Cartesian frame, with ξ_1, ξ_2, and ξ_3 being the corresponding coordinates, and $f_{/3}$ denotes the partial derivative of f with respect to ξ_3.

As a notation rule, subscript o identifies quantities in the initial configuration (i.e., at $\tau = 0$), subscript k will take values in $\{1, 2\}$, and j in $\{1, 2, 3\}$. Finally, $H_a(x)$ denotes the Heaviside function centered at $x = a$, with $H_a(x) = 0$ for $x \leq a$ and $H_a(x) = 1$ for $x > a$.

After the description of fibril elasto-damage mechanisms that are herein addressed (see Sect. 2.1), the multiscale approach introduced by Marino and Vairo (2014a) in the MV-model is described in Sect. 2.2. Then, in the following Sects. 2.3 and 2.4, fibril and RUS model are, respectively, presented together with their coupling terms.

2.1 Evidence-based elasto-damage mechanisms

At fibril scale and starting from experimental observations, two *in-series* deformation mechanisms are introduced analogously to the MV-model. In fact, fibril strain can be experimentally measured by means of both small-angle and wide-angle X-ray diffraction patterns (Sasaki and Odajima 1996). In the latter case, when employing a reflection corresponding to the distance of few nanometers, a lower value of fibril strain is obtained with respect to the one obtained through small-angle X-rays (Sasaki and Odajima 1996). This evidence indicates that fibril deformation is governed at least by two distinct mechanisms.

Moreover, in order to account for the variability of yielding-like and brittle-like failure mechanisms observed for fibrils, (Svensson et al. 2013), three damage mechanisms are introduced: a perfectly-yielding behavior (yielding at constant stress), yielding with softening, and a brittle-like behavior. This choice generalizes the MV-model where only two fibril damage mechanisms were introduced allowing for the description only of either perfectly-yielding/softening-yielding or perfectly-yielding/brittle behaviors.

At nanoscale, starting from experimental and atomistic evidence and analogously to the MV-model, present model accounts for

- slip-pulse (SP): localized breaking of weak cross-links and their continuous reactivation among adjacent residues during molecular sliding (Buehler 2006);
- the delayed activation of enzymatic cross-links: the latter can indeed transmit the force and hold back molecular sliding only when the hook-shaped cross-linked telopeptide straightens out (Uzel and Buehler 2011; Depalle et al. 2014);
- interstrand delamination (ID): a polypeptide strand within a collagen molecule slides with respect to the other two because the force transmitted through the covalent cross-link (acting upon a single strand) breaks the weak bonds inside the triple-helix structure. Accordingly, a strand pull-out mechanism altering molecular quaternary structure is promoted, (Buehler 2006; Uzel and Buehler 2011).

Moreover, as an enhancement with respect to the MV-model, further nanoscale mechanisms are accounted for:

- the nonlinear coupling of entropic and energetic molecular deformation mechanisms (Buehler and Wong 2007; Fratzl 2008; Maceri et al. 2012b);
- molecular covalent bond rupture (MR): molecular damage associated with the breaking of covalent bonds within the polypeptide strands (Buehler 2006; Maceri et al. 2012b);
- a distinct behavior for mature and immature enzymatic cross-links (Depalle et al. 2014);
- a refined and nonlinear activation rate for slip-pulse mechanisms.

Figure 2 represents a schematic representation of the elasto-damage internal mechanisms at nanoscale that are herein addressed for describing fibril mesoscale constitutive response.

As interscale relationships and in agreement with Sasaki and Odajima (1996), the deformation mechanism associated with wide-angle X-ray diffraction is related to molecular elongation mechanisms because this technique allows to measure strains associated with the distance between neighboring amino acids along the collagen helix. Accordingly, the second deformation mechanism (the difference between the deformations associated with small-angle and wide-angle X-ray diffraction) is associated with molecular sliding.

Finally, fibril perfectly-yielding behavior is associated with SP (Buehler 2006; Uzel and Buehler 2011), softening-yielding failure with ID (Buehler 2006; Uzel and Buehler 2011), and brittle rupture with MR (Buehler 2006; Buehler and Wong 2007; Buehler 2008; Svensson et al. 2013).

2.2 Marino–Vairo's multiscale approach

A collagen fibril in the actual configuration (at $\tau = t$) is regarded as a right circular cylinder $\mathcal{F}$ of radius r_f (assumed to be constant in time) and length ℓ_f (assumed to be variable in time), whose axis is $\boldsymbol{\xi}_3$. Thereby,

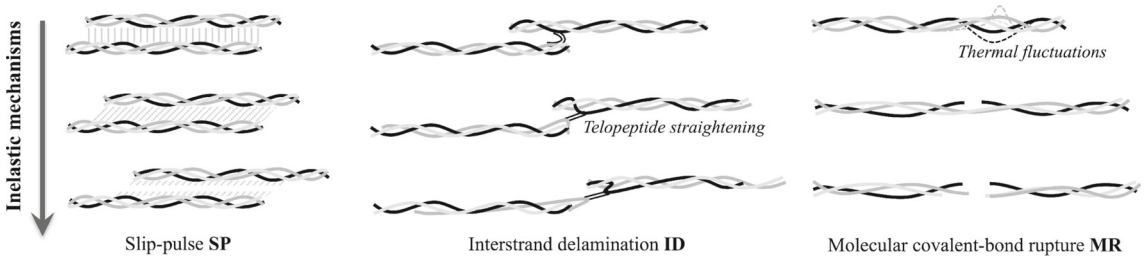

Fig. 2 Evidence-based fibril internal elasto-damage mechanisms. *Left* Molecular sliding related to slip-pulse (SP). *Center* Delayed activation of enzymatic covalent cross-links (both mature and immature) due to the straightening of the cross-linked telopeptide; interstrand delamination (ID) associated with a strand pull-out mechanism. *Right* Nonlinear molecular elasticity related to entropic (thermal fluctuations) and energetic (triple-helix uncoiling and stretching of molecular backbone) mechanisms; molecular covalent bond rupture (MR)

$$\mathcal{F} = \left\{(\xi_1, \xi_2, \xi_3) \in A_f \times \left[0, \ell_f\right]\right\},$$

where $A_f = \{(\xi_1, \xi_2) \,|\, \xi_1^2 + \xi_2^2 \leq r_f^2\}$ is the fibril cross-sectional domain, whose constant measure is $\mathcal{A}_f = \pi r_f^2$.

Collagen molecules in the actual configuration are regarded, in turn, as cylinder-like sub-domains whose axes are aligned with the fibril's one and whose measures of cross-sectional area, length and volume are denoted by $\mathcal{A}_m$ (assumed to be constant in time), ℓ_m (assumed to be variable in time), and $\Omega_m = \mathcal{A}_m \ell_m$, respectively.

The choice of employing a cylindrical shape for both molecules and fibrils is done in order to maintain the model simple and, thereby, to allow for an effective upscaling toward macroscale tissue mechanical modeling. Nevertheless, thanks to refined expressions of interscale compatibility relationships and constitutive laws in Sect. 2.4, dominant mechanisms related to the non-cylindrical geometry of fibril constituents are properly described. Results, shown in Sect. 3, highlight that this approach is effective for capturing essential nonlinear mechanisms of nanoscale constituents that affect fibril mechanics.

With reference to the initial configuration (at time $\tau = 0$), average quantities describing the molecular arrangement within fibrils are introduced (Marino and Vairo 2014a):

- $\mathcal{O}_c(\xi_1, \xi_2)$: molecular density along the $\boldsymbol{\xi}_3$-direction;
- $\mathcal{A}_c = \int_{A_f} \mathcal{O}_c(\xi_1, \xi_2) d\xi_1 d\xi_2$: average load-bearing area;
- $n_s = \ell_{f,o}/\ell_{m,o}$: average molecular number along ξ_3;
- $n_a = \mathcal{A}_c/\mathcal{A}_m$: average molecular number in A_f;
- λ_c^T: average number of trivalent mature cross-links per collagen molecule.
- λ_c^D: average number of divalent immature cross-links per collagen molecule.

Fibril deformation and damage behavior are obtained by introducing a suitable set of state variables $\mathcal{S}_f = \{S_f^j \text{ with } j = 1, \ldots, M_f\}$ that describes the mechanisms observed at the mesoscale. Dual to $\mathcal{S}_f$, there exist static quantities whose equilibrium relationships among themselves and with external actions can be straight obtained by means of the application of the principle of virtual power (PVP, Frémond 2002; Marino 2013).

Fibril elasto-damage response is obtained from equilibrium equations solved by employing suitable constitutive laws, namely relationships between state quantities and the corresponding dual static quantities. Denoting with $\dot{\mathcal{S}}_f$ the set collecting the time derivatives of $\mathcal{S}_f$ and following Frémond (2002), constitutive laws are obtained by subdifferentiation of fibril free energy $\psi_f = \psi_f(\mathcal{S}_f)$ (with the unit of work per unit length) and pseudo-potential of dissipation $\phi_f = \phi_f(\dot{\mathcal{S}}_f)$ (with the unit of power per unit length). These functions are defined by adopting a multiscale rationale based on the detailed description of fibril constituents' behavior and employing the definition of the RUS.

Fibril RUS is herein chosen as: one collagen molecule ($\mathcal{M}$); λ_c^T and λ_c^D covalent cross-links among $\mathcal{M}$ and surrounding molecules; a linear density of weak interactions among $\mathcal{M}$ and surrounding molecules, constant along the length of $\mathcal{M}$.

Then, the RUS is described by introducing nanoscale state variables collected in $\mathcal{S}_R = \{\mathcal{S}_m, \mathcal{S}_c, \mathcal{S}_w\}$, where $\mathcal{S}_m = \{s_m^n \text{ with } n = 1, \ldots, M_m\}$, $\mathcal{S}_c = \{s_c^n \text{ with } n = 1, \ldots, M_c\}$ and $\mathcal{S}_w = \{s_w^n \text{ with } n = 1, \ldots, M_w\}$ are the sets of the state variables describing $\mathcal{M}$, covalent cross-links (both mature and immature) and intermolecular weak bonds, respectively. Deformation and damage at the fibril's scale are related to nanoscale mechanisms within the RUS by introducing interscale compatibility relationships between $\mathcal{S}_R$ and $\mathcal{S}_f$. Nanoscale state variables are assumed to be constant within a single RUS (hence, modeled as a zero-dimensional domain) and in A_f, but they can depend on ξ_3 when referred to RUSs located at different values of ξ_3.

Mechanics of nanoscale constituents of the RUS is, in turn, described by means of free energies $\Psi_m(\mathcal{S}_m)$, $\mathcal{E}_c^T(\mathcal{S}_c)$, $\mathcal{E}_c^D(\mathcal{S}_c)$, $\mathcal{E}_w(\mathcal{S}_w)$, and pseudo-potential of dissipation $\Phi_m(\dot{\mathcal{S}}_m)$, $\mathcal{D}_c^T(\dot{\mathcal{S}}_c)$, $\mathcal{D}_c^D(\dot{\mathcal{S}}_c)$, $\mathcal{D}_w(\dot{\mathcal{S}}_w)$ for molecules, mature covalent cross-links, immature covalent cross-links, and intermolecular weak bonds, respectively.

Accordingly, RUS free energy (with the unit of work per unit length) is defined as

$$\psi_R|_{\mathcal{S}_R} := \bar{\psi}_R + \frac{1}{\ell_{m,o}}\left(d\mathcal{E}_R^m + \lambda_c^T d\mathcal{E}_R^T + \lambda_c^D d\mathcal{E}_R^D + d\mathcal{E}_R^w\right),$$
$$d\mathcal{E}_R^m := \Omega_{m,o}\, f_m \boxtimes d\mathcal{S}_f\big|_{\mathcal{S}_m}, \quad d\mathcal{E}_R^T := F_c^T \boxtimes d\mathcal{S}_f\Big|_{\mathcal{S}_c},$$
$$d\mathcal{E}_R^D := F_c^D \boxtimes d\mathcal{S}_f\Big|_{\mathcal{S}_c}, \qquad d\mathcal{E}_R^w := F_w \boxtimes d\mathcal{S}_f|_{\mathcal{S}_w},$$

where $\bar{\psi}_R = \psi_R|_{\tau=\bar{t}}$ is RUS reference free energy,

$$f_m \boxtimes d\mathcal{S}_f|_{\mathcal{S}_m} := \sum_{j=1}^{M_f}\sum_{n=1}^{M_m} p_{nj}, \quad \text{with}$$
$$p_{nj} = \begin{cases} \frac{\partial \Psi_m}{\partial s_m^n}\Big|_{\mathcal{S}_m} \cdot dS_f^j\Big|_{\mathcal{S}_R} & \text{if } s_m^n = s_m^n(S_f^j) \\ 0 & \text{else} \end{cases}, \tag{1}$$

and where an analogous notation holds for the term involving F_c^T (resp., F_c^D and F_w) by employing $s_c^n, \mathcal{S}_c, M_c, \mathcal{E}_c^T$ (resp., $s_c^n, \mathcal{S}_c, M_c, \mathcal{E}_c^D$, and $s_w^n, \mathcal{S}_w, M_w, \mathcal{E}_w$) instead of $s_m^n, \mathcal{S}_m, M_m, \Psi_m$.

Thereby, fibril free energy is defined as

$$\psi_f\big|_{\mathcal{S}_f} := \frac{1}{\mathcal{A}_m}\int_{A_f} \psi_R|_{\mathcal{S}_R}\, \mathcal{O}_c(\xi_1,\xi_2)\, d\xi_1\, d\xi_2 + \mathcal{I}_d|_{\mathcal{S}_f}$$
$$= n_a\, \psi_R|_{\mathcal{S}_R} + \mathcal{I}_d|_{\mathcal{S}_f}, \tag{2}$$

where $\mathcal{I}_d$ is an interaction free-energy contribution.

Finally, RUS pseudo-potential of dissipation is defined as

$$\phi_R|_{\dot{\mathcal{S}}_R} := \frac{1}{\ell_{m,o}}\left(\Omega_{m,o}\Phi_m + \lambda_c^T \mathcal{D}_c^T + \lambda_c^D \mathcal{D}_c^D + \mathcal{D}_w\right)\Big|_{\dot{\mathcal{S}}_R},$$

and fibril pseudo-potential of dissipation is

$$\phi_f\big|_{\dot{\mathcal{S}}_f} := \frac{1}{\mathcal{A}_m}\int_{A_f} \phi_R|_{\dot{\mathcal{S}}_R}\, \mathcal{O}_c(\xi_1,\xi_2)\, d\xi_1\, d\xi_2$$
$$= n_a\, \phi_R|_{\dot{\mathcal{S}}_R}. \tag{3}$$

2.3 Fibril model

Since fibrils mainly undergo uniaxial traction, fibril deformation at mesoscale is described by introducing centerline axial displacement $u = u(\xi_3)$ which can be observed through small-angle X-ray diffraction. As previously described and following experimental evidence (see Sect. 2.1), the two in-series mechanisms, contributing to fibril axial deformation, are described by

- u_1, related to wide-angle X-ray diffraction,
- u_2, related to the difference between small-angle and wide-angle X-ray diffraction,

with $du_1 + du_2 = du$. In agreement with classical bar's theories, natural strain measures e_1 and e_2 are introduced, by defining their perturbations as $de_1 = du_{1/3}$ and $de_2 = du_{2/3}$.

Fibril damage is described by means of variables

- $\beta_1(\xi_3)$ and $\gamma_1(\xi_3)$, related to yielding with softening,
- $\beta_2(\xi_3)$ and $\gamma_2(\xi_3)$, related to perfectly yielding behavior,
- $\beta_3(\xi_3)$ and $\gamma_3(\xi_3)$, related to a brittle behavior,

with β_j valued in $[0, 1]$, where $\beta_j = 1$ means that the damage mechanism is not activated and $\beta_j = 0$ that it is fully activated. Variables γ_j are introduced to describe damage diffusion, by defining $\gamma_j = \beta_{j/3}$.

Accordingly, fibril state variables are

$$\mathcal{S}_f := \{e_k, \beta_j, \gamma_j\}. \tag{4}$$

The static quantities associated with $\mathcal{S}_f$ are the normal forces $N_k = N_k(\xi_3)$ (dual to e_k), the sub-mesoscale damage forces $b_j = b_j(\xi_3)$ (dual to β_j), and the sub-mesoscale damage works $h_j = h_j(\xi_3)$ (dual to γ_j).

Consider $u|_{\xi_3=0} = 0$ as a displacement boundary condition, and let the fibril be loaded by the force $\mathbf{F} = F_f \boldsymbol{\xi}_3$ at $\xi_3 = \ell_f$ and by the axial force density $\mathbf{q}(\xi_3) = q_f(\xi_3)\boldsymbol{\xi}_3$. Moreover, let $a_f = a_f(\xi_3)$ be a non-mechanical source of damage (e.g., biochemical, electrical, magnetic) distributed along the fibril length. Accordingly, through the application of the PVP (Marino 2013; Marino and Vairo 2014a), the equations governing the equilibrium of the afore-introduced static quantities are:

$$N_{k/3} = -q_f \ \text{ for } \ \xi_3 \in [0, \ell_f], \tag{5a}$$
$$h_{j/3} - b_j = a_f \ \text{ for } \ \xi_3 \in [0, \ell_f], \tag{5b}$$

with boundary conditions:

$$N_k|_{\xi_3=\ell_f} = F_f\ ,\ N_1|_{\xi_3=0} = N_2|_{\xi_3=0}\,, \tag{5c}$$
$$h_j|_{\xi_3=0} = h_j|_{\xi_3=\ell_f} = 0. \tag{5d}$$

Finally, constitutive laws are:

$$N_k := \frac{\partial \psi_f}{\partial e_k} + \frac{\partial \phi_f}{\partial \dot{e}_k}, \tag{6a}$$
$$b_j := \frac{\partial \psi_f}{\partial \beta_j} + \frac{\partial \phi_f}{\partial \dot{\beta}_j}, \tag{6b}$$
$$h_j := \frac{\partial \psi_f}{\partial \gamma_j} + \frac{\partial \phi_f}{\partial \dot{\gamma}_j}. \tag{6c}$$

Following Eq. (2), only the interaction free-energy contribution has to be defined at the fibril scale, and it is herein chosen as:

$$\mathcal{I}_d\left(\gamma_1,\gamma_2,\gamma_3\right) := \left(k_1\gamma_1^2 + k_2\gamma_2^2 + k_3\gamma_3^2\right)/2, \tag{7}$$

where k_j denotes damage diffusion coefficient. The other quantities for the definition of ψ_f and ϕ_f as in Eqs. (2) and (3) will straightly derive from the nanoscale model, described in what follows.

2.4 RUS model

Before introducing RUS state variables, some auxiliary quantities are conveniently introduced: molecular nominal strain measure $\varepsilon_m = \ell_m/\ell_{m,o} - 1$ ($\ell_{m,o}$ being molecular length at $\tau = 0$) and molecular sway δ. Accordingly, actual RUS length is $\ell_R = \ell_m + \delta$ (with $\ell_{R,o} = \ell_{m,o}$ being RUS length at $\tau = 0$) and nominal strain is described by $\varepsilon_R = \ell_R/\ell_{R,o} - 1 = \varepsilon_m + \varepsilon_{CL}$ where $\varepsilon_{CL} = \delta/\ell_{m,o}$.

Moreover, two contributions for molecular sliding are introduced: δ_w, being molecular sway associated with weak bonds deformation, and δ_c, being molecular sway associated with covalent bonds deformation. In detail, it results:

$$d\delta_w := d\delta, \quad d\delta_c := f_c(\bar{\delta})d\delta, \tag{8a}$$

being

$$f_c(x) := \frac{1}{\left[1 + e^{-2\mu(x-\delta_o)}\right]} \xrightarrow[\mu\to+\infty]{} H_{\delta_o}(x), \tag{8b}$$

the activation function of covalent cross-links. Thereby, two parameters have been introduced: $\mu \in \mathbb{R}^+$ is an activation shape parameter and δ_o is a measure of the molecular sway inducing the telopeptide straightening, responsible for the delayed activation of the covalent cross-link stretch (Uzel and Buehler 2011; Marino and Vairo 2014a).

The deformation of covalent cross-links is assumed to be elastic and thereby fully recovered upon loading removal. Mature and immature cross-links are assumed to act as *in-parallel*, and thereby they can be described introducing a unique strain measure. The deformation of both weak cross-links and molecules is regarded as the series of elastic (denoted by superscript e) and inelastic contributions. Inelastic contributions are not recovered upon unloading: plastic-like mechanisms (denoted by superscript p) are associated with residual strains due to either SP or ID; brittle-like mechanisms (denoted by superscript b) are associated with molecular fracture due to MR. Damage of molecular structural integrity (namely, ID and MR) is associated with relaxation mechanisms (that is, a decay of elastic strain with time).

Accordingly, the RUS elasto-damage mechanisms are herein described by

- for weak cross-links:
  - the elastic weak-related molecular sliding δ_w^e, or equivalently $\varepsilon_w^e = \delta_w^e/\ell_{m,o}$;
  - the SP-inelastic weak-related molecular sliding δ_w^p, or equivalently $\varepsilon_w^p = \delta_w^p/\ell_{m,o}$;
  - damage parameter β_w associated with the rupture of intermolecular weak bonds and thereby with SP;
- for covalent cross-links:
  - the elastic covalent-related molecular sliding $\varepsilon_c = \delta_c/\ell_{m,o}$;
- for collagen molecules:
  - the elastic molecular strain ε_m^e;
  - the ID-inelastic molecular strain ε_m^p associated with a molecular relaxation mechanism governed by the decay time constant τ_o^{ID};
  - the MR-inelastic molecular strain ε_m^b associated with a molecular relaxation mechanism governed by the decay time constant τ_o^{MR};
  - damage parameter β_d associated with the rupture of molecular interstrand weak bonds and thereby with ID;
  - damage parameter β_m associated with the rupture of molecular intrastrand covalent bonds and thereby with MR.

With respect to the MV-model, ε_m^b and β_m enrich molecular description. In detail, when $\beta_m = 1$, intramolecular covalent bonds are considered to be sound, possible molecular strain increment is either elastic or ID-inelastic (depending on the value of β_d), and MR-inelastic strain is not activated (that is, $\dot{\varepsilon}_m^b = 0$); when $\beta_m = 0$, intramolecular covalent bonds are considered to be totally broken, and possible molecular strain increment is neither elastic nor ID-inelastic (that is, $\dot{\varepsilon}_m^e = \dot{\varepsilon}_m^p = 0$); when $0 < \beta_m < 1$, intramolecular covalent bonds are considered to be partially broken, and elastic, ID-inelastic and MR-inelastic mechanisms may occur.

The relationships between ε_m^p and β_d and between ε_w^p and β_w are analogous to the one previously described for ε_m^b and β_m (Marino and Vairo 2014a).

In Fig. 3, nanoscale elasto-damage mechanisms described by present model are schematically represented. In summary, RUS state variables are herein chosen as:

$$\mathcal{S}_m := \left\{\varepsilon_m^e, \varepsilon_m^p, \varepsilon_m^b, \beta_d, \beta_m\right\}, \quad \mathcal{S}_w := \left\{\varepsilon_w^e, \varepsilon_w^p, \beta_w\right\},$$
$$\mathcal{S}_c := \left\{\varepsilon_c\right\}.$$

2.4.1 Constitutive models at the nanoscale

Constitutive choices are introduced by following an internal constrained approach. Physical restrictions are introduced

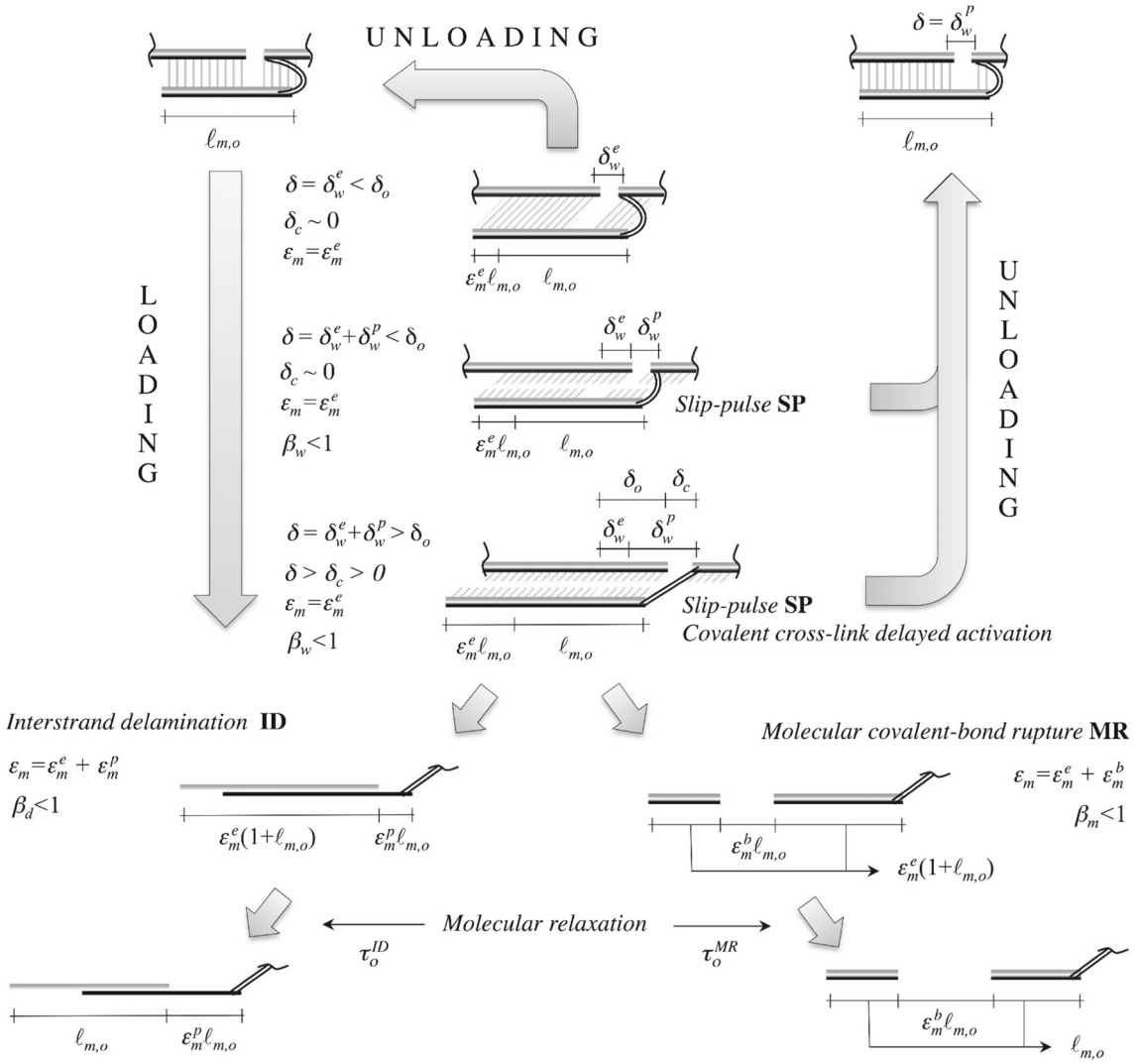

Fig. 3 Elasto-damage nanoscale mechanisms in fibrils. Sketch of modeling assumptions on state variables in a representative unit system (RUS)

directly in the variational formulation by means of suitable indicator functions and employing arguments from convex analysis (see Appendix section "Basics of convex analysis").

Similar to the MV-model, covalent cross-links are assumed to behave as linearly elastic. Trivalent mature (superscript T) and divalent immature (superscript D) cross-links are described by:

$$\mathcal{E}_c^T(\varepsilon_c) := \frac{K_c^T \varepsilon_c^2}{2}, \quad \mathcal{E}_c^D(\varepsilon_c) := \frac{K_c^D \varepsilon_c^2}{2}, \tag{9a}$$

$$\mathcal{D}_c^T := 0, \quad \mathcal{D}_c^D := 0, \tag{9b}$$

where $K_c^T = k_c^T \ell_{m,o}^2$, $K_c^D = k_c^D \ell_{m,o}^2$, and k_c^T (resp., k_c^D) is the mature (resp., immature) covalent cross-link stiffness.

The mechanics of weak cross-links is herein described by defining

$$\mathcal{E}_w(\varepsilon_w^e, \beta_w) := \mathcal{E}_w^{el}(\varepsilon_w^e) + \beta_w \mathcal{E}_w^{sp} + (1-\beta_w) w_w + \\ + \mathrm{I}_{[0,1]}(\beta_w), \tag{10a}$$

$$\mathcal{D}_w(\dot{\beta}_w) := \frac{c_w}{2}\dot{\beta}_w^2 + \mathrm{I}^+(\dot{\beta}_w + \bar{\beta}_w^{\omega} v_w), \tag{10b}$$

where $\mathcal{E}_w^{el}(\varepsilon_w^e) = K_w[\varepsilon_w^e]^2/2$ is the weak-bonds elastic energy, with $K_w = k_w \ell_{m,o}^2$, k_w is the weak-bond stiffness, w_w and c_w are the activation threshold and viscosity of intermolecular weak-bonds damage, respectively. Moreover, $\mathrm{I}_{[0,1]}$ is introduced to enforce as an internal constraint the restriction $\beta_w \in [0, 1]$, and $\mathcal{E}_w^{sp}$ is the free-energy part contributing to SP, here chosen as $\mathcal{E}_w^{sp} = \mathcal{E}_w^{el}(\bar{\varepsilon}_w^e)$. The aforementioned terms correspond to the ones proposed in the MV-model. Nevertheless, a new term is here introduced, namely

- $\mathrm{I}^+(\dot{\beta}_w + \bar{\beta}_w^{\omega} v_w)$ with $v_w, \omega \in \mathbb{R}^+$ that enforces the restriction

$$\dot{\beta}_w \geq -\bar{\beta}_w^{\omega} v_w. \tag{11}$$

Accordingly, a controlled activation rate of slip-pulse, nonlinearly depending on damage amount, is introduced. Results will clearly show that this choice straightly follows from experimental data. It is also worth pointing out that no upper bound for damage rate of weak bonds is introduced and thereby damage evolution can be lower or higher than zero (namely, damage is reversible). Accordingly, weak cross-links may break and reform.

Constitutive response of $\mathcal{M}$ is defined by:

$$\begin{aligned}\Psi_m\left(\varepsilon_m^e, \beta_d, \beta_m\right) := {} & \Psi_m^{el}\left(\varepsilon_m^e\right) + \beta_d \Psi_m^{ID} + \beta_m \Psi_m^b + \\ & + \left(1-\beta_d\right) w_d + \left(1-\beta_m\right) w_m + \\ & + \mathrm{I}_{[0,1]}\left(\beta_d\right) + \mathrm{I}_{[0,1]}\left(\beta_m\right), \end{aligned} \tag{12a}$$

$$\Phi_m\left(\dot{\beta}_d, \dot{\beta}_m\right) := \frac{c_d \dot{\beta}_d^2}{2} + \frac{c_m \dot{\beta}_m^2}{2} + \mathrm{I}_{[-v_m,0]}\left(\dot{\beta}_m\right). \tag{12b}$$

Analogously to the MV-model, intramolecular hydrogen-bonds damage is governed by threshold w_d, viscosity c_d, and free-energy part contributing to damage onset Ψ_m^{ID}. Introducing

$$\tilde{\varepsilon}_c := \max_{\tau\in[0,\bar{t}]} \left\{\varepsilon_c(\tau)\right\}, \tag{12c}$$

and in order to account for mature and immature cross-links, Ψ_m^{ID} is assumed to be:

$$\Psi_m^{ID} := \frac{H_0\left(\lambda_c^T\right)\mathcal{E}_c^T\left(\tilde{\varepsilon}_c\right) + H_0\left(\lambda_c^D\right)\mathcal{E}_c^D\left(\tilde{\varepsilon}_c\right)}{\Omega_{m,o}}. \tag{12d}$$

No restrictions are introduced for ID damage rate.

Moreover, new terms are introduced in the present paper for the refined modeling of molecular behavior

- the activation threshold w_m and viscosity c_m of intramolecular covalent bonds damage;
- $\mathrm{I}_{[-v_m,0]}(\dot{\beta}_m)$ with $v_m \in \mathbb{R}^+$, introduced to enforce the restriction $\dot{\beta}_m \leq 0$, that is molecular damage is irreversible, but also that maximum damage rate is limited, namely $\dot{\beta}_m \geq -v_m$, as previously shown by Maceri et al. (2012b);
- the nonlinearly elastic free-energy contribution Ψ_m^e,

$$\Psi_m^e\left(\varepsilon_m^e\right) := \bar{\Psi}_m^e + \bar{\sigma}_m d\varepsilon_m^e + \frac{E_m\left(\bar{\varepsilon}_m^e\right)\left[d\varepsilon_m^e\right]^2}{2}, \tag{13}$$

from which elastic molecular stress results

$$\sigma_m\left(\varepsilon_m^e\right) := \frac{\partial \Psi_m^e}{\partial d\varepsilon_m^e} = \bar{\sigma}_m + E_m\left(\bar{\varepsilon}_m^e\right) d\varepsilon_m^e, \tag{14}$$

and where $\bar{\Psi}_m^e = \Psi_m^e|_{\tau=\bar{t}}$, $\bar{\sigma}_m = \sigma_m|_{\tau=\bar{t}}$, and function $E_m(\varepsilon_m^e)$ is the molecular tangent elastic modulus, depending on entropic–energetic *in-series* mechanisms (Maceri et al. 2012b). The entropic mechanism is associated with strain contribution $\varepsilon_m^{e,s}$ and tangent modulus $E_m^s(\varepsilon_m^{e,s})$, the energetic mechanism with strain $\varepsilon_m^{e,h}$ and modulus $E_m^h(\varepsilon_m^{e,h})$. Accordingly, E_m is defined as

$$E_m\left(\varepsilon_m^e\right) := \frac{E_m^s\left(\varepsilon_m^{e,s}\right) E_m^h\left(\varepsilon_m^{e,h}\right)}{E_m^s\left(\varepsilon_m^{e,s}\right) + E_m^h\left(\varepsilon_m^{e,h}\right)}, \tag{15a}$$

where $\varepsilon_m^{e,s}$ and $\varepsilon_m^{e,h}$ are obtained from solving the following differential problem:

$$\dot{\varepsilon}_m^{e,s} = \frac{E_m\left(\varepsilon_m^e\right)\dot{\varepsilon}_m^e}{E_m^s\left(\varepsilon_m^{e,s}\right)}, \quad \dot{\varepsilon}_m^{e,h} = \frac{E_m\left(\varepsilon_m^e\right)\dot{\varepsilon}_m^e}{E_m^h\left(\varepsilon_m^{e,h}\right)}. \tag{15b}$$

Entropic stiffness E_m^s models thermal fluctuations by recovering the well-established worm-like chain model (Marko and Siggia 1995; Maceri et al. 2012b), and it is defined as

$$E_m^s\left(\varepsilon_m^{e,s}\right) := \frac{k_B T}{\mathcal{A}_m \ell_p}\left\{\frac{r_\ell}{2\left[1-r_\ell\left(1+\varepsilon_m^{e,s}\right)\right]^3} + r_\ell\right\}, \tag{15c}$$

where k_B is the Boltzmann constant, T the absolute temperature, ℓ_p molecular persistence length, and $r_\ell = \ell_{m,o}/\ell_c$ with ℓ_c the molecular contour length. Finally, E_m^h models triple-helix uncoiling and stretching of molecular backbone (Buehler 2006; Maceri et al. 2012b), and it is defined as

$$E_m^h\left(\varepsilon_m^{e,h}\right) := \frac{\hat{E} r_\ell}{1+e^{-\eta\left(r_\ell \varepsilon_m^{e,h} - \varepsilon_o^h\right)}} + \hat{E}_o r_\ell, \tag{15d}$$

where $\hat{E}$, $\hat{E}_o$, ε_o^h, and η are model parameters associated with the uncoiling of the triple-helix collagen structure.

- Ψ_m^b: free-energy part contributing to damage of intramolecular covalent bonds, herein chosen as

$$\Psi_m^b := \Psi_m^e\left(\tilde{\varepsilon}_m^e\right) \quad \text{with} \quad \tilde{\varepsilon}_m^e := \max_{\tau\in[0,\bar{t}]}\left\{\varepsilon_m^e(\tau)\right\}. \tag{16}$$

2.5 Interscale compatibility relationships

Nanoscale state variables in $\mathcal{S}_R$ are related to the fibril's, $\mathcal{S}_f$, by means of incremental interscale compatibility relationships in agreement with the afore-described interscale evidence (see Sect. 2.1).

Firstly, let the following convenient control functions be introduced

$$\alpha_k := \left(1-\bar{\beta}_k\right) H_0\left(du_k\right), \quad \nu_k := 1-\alpha_k, \quad \alpha_3 := 1-\bar{\beta}_3.$$

The first mesoscale deformation mode e_1 is associated with molecular elongation through

$$d\varepsilon_m^e := \bar{\beta}_3\left[\nu_1\frac{\bar{\ell}_R}{\ell_{m,o}}de_1-\alpha_1\frac{\bar{\varepsilon}_m^e d\tau}{\tau_o^{ID}}\right]-\alpha_3\frac{\bar{\varepsilon}_m^e d\tau}{\tau_o^{MR}}, \tag{17a}$$

$$d\varepsilon_m^p := \bar{\beta}_3\left[\alpha_1\frac{\bar{\ell}_R}{\ell_{m,o}}de_1+\alpha_1\frac{\bar{\varepsilon}_m^e d\tau}{\tau_o^{ID}}\right], \tag{17b}$$

$$d\varepsilon_m^b := \alpha_3\left[\frac{\bar{\ell}_R}{\ell_{m,o}}de_1+\frac{\bar{\varepsilon}_m^e d\tau}{\tau_o^{MR}}\right], \tag{17c}$$

resulting

$$d\varepsilon_m = d\varepsilon_m^e + d\varepsilon_m^p + d\varepsilon_m^b = \frac{\bar{\ell}_R}{\ell_{m,o}}de_1.$$

On the other hand, the second mesoscale deformation mode e_2 is associated with molecular sway by choosing $d\delta = \ell_{m,o}d\varepsilon_{CL} = \bar{\ell}_R de_2$ and, distinguishing the different mechanisms,

$$\ell_{m,o}d\varepsilon_w^e := [1-\alpha_2]\,\bar{\ell}_R de_2 = \nu_2\bar{\ell}_R de_2, \tag{18a}$$

$$\ell_{m,o}d\varepsilon_w^p := \alpha_2\bar{\ell}_R de_2, \tag{18b}$$

$$\ell_{m,o}d\varepsilon_c := \bar{\ell}_R f_c(\bar{\delta})de_2 \xrightarrow[\mu\to+\infty]{} \bar{\ell}_R H_{\delta_o}(\bar{\delta})de_2. \tag{18c}$$

Thereby, since $d\delta_w = \ell_{m,o}(d\varepsilon_w^e + d\varepsilon_w^p)$ and $d\delta_c = \ell_{m,o}d\varepsilon_c$,

$$d\delta_w = \bar{\ell}_R de_2 = d\delta, \quad d\delta_c \le \bar{\ell}_R de_2 = d\delta. \tag{19}$$

Finally, fibril and nanoscale damage perturbations are related each other as

$$d\beta_d := d\beta_1, \quad d\beta_w := d\beta_2, \quad d\beta_m := d\beta_3. \tag{20}$$

2.6 Governing equations

For obtaining an expression for fibril free energy within the present multiscale framework, it is firstly worth pointing out that $\mathcal{E}_c^T = \mathcal{E}_c^T(\varepsilon_c)$ and $\mathcal{E}_c^D = \mathcal{E}_c^D(\varepsilon_c)$ from Eq. (9a), $\mathcal{E}_w = \mathcal{E}_w(\varepsilon_w^e, \beta_w)$ from Eq. (10a), and $\Psi_m = \Psi_m(\varepsilon_m^e, \beta_d, \beta_m)$ from Eq. (12a). Accordingly, among the full set of interscale compatibility relationships, the functional dependencies $\varepsilon_m^e = \varepsilon_m^e(e_1)$ from Eq. (17a), $\varepsilon_w^e = \varepsilon_w^e(e_2)$ from Eq. (18a), $\varepsilon_c = \varepsilon_c(e_2)$ from Eq. (18c), $\beta_d = \beta_1$, $\beta_w = \beta_2$, and $\beta_m = \beta_3$ from Eq. (20) are highlighted for deriving constitutive relationships. Moreover, it is noted that, in the present incremental formulation, the derivative with respect to a given quantity (e.g., x) corresponds to the derivative with respect to its perturbation (namely, dx).

Based on the definition (1) and on previous consideration, fibril free energy in Eq. (2) results equal to

$$\begin{aligned}\psi_f = \frac{\mathcal{A}_c}{\mathcal{A}_m}\Bigg[\bar{\psi}_R+\mathcal{A}_m\left(\frac{\partial\Psi_m}{\partial\varepsilon_m^e}de_1+\frac{\partial\Psi_m}{\partial\beta_d}d\beta_1+\frac{\partial\Psi_m}{\partial\beta_m}d\beta_3\right)+\\ +\frac{1}{\ell_{m,o}}\left(\lambda_c^T\frac{\partial\mathcal{E}_c^T}{\partial\varepsilon_c}+\lambda_c^D\frac{\partial\mathcal{E}_c^D}{\partial\varepsilon_c}+\frac{\partial\mathcal{E}_w}{\partial\varepsilon_w^e}\right)de_2+\frac{\partial\mathcal{E}_w}{\partial\beta_w}d\beta_2\Bigg]+\\ +\frac{1}{2}\left(k_1\beta_{1/3}^2+k_2\beta_{2/3}^2+k_3\beta_{3/3}^2\right),\end{aligned} \tag{21}$$

where Eq. (7) has been employed. Moreover, from Eqs. (9b), (10b), and (12b), pseudo-potential of dissipation ϕ_f in Eq. (3) straight results equal to

$$\phi_f = \frac{\mathcal{A}_c}{\mathcal{A}_m}\left[\mathcal{A}_m\Phi_m\left(\dot{\beta}_1,\dot{\beta}_3\right)+\frac{1}{\ell_{m,o}}\mathcal{D}_w\left(\dot{\beta}_2\right)\right]. \tag{22}$$

Accordingly, from Eqs. (6a) and (21), fibril axial forces are:

$$\frac{N_1}{\mathcal{A}_c} = \frac{\partial\Psi_m}{\partial\varepsilon_m^e} = \frac{\partial\Psi_m^e}{\partial d\varepsilon_m^e} = \bar{\sigma}_m + \bar{E}_m d\varepsilon_m^e, \tag{23a}$$

$$\frac{N_2}{n_a} = \frac{1}{\ell_{m,o}}\left[\lambda_c^T\frac{\partial\mathcal{E}_c^T}{\partial\varepsilon_c}+\lambda_c^D\frac{\partial\mathcal{E}_c^D}{\partial\varepsilon_c}+\frac{\partial\mathcal{E}_w}{\partial\varepsilon_w^e}\right] = k_c^{eq}\delta_c + k_w\delta_w^e, \tag{23b}$$

where $\bar{E}_m = E_m(\bar{\varepsilon}_m^e)$ and $k_c^{eq} = \lambda_c^T k_c^T + \lambda_c^D k_c^D$. Moreover, from Eqs. (6b), (6c) and (22), static quantities associated with fibril damage are

$$\frac{b_1}{\mathcal{A}_c} \in \frac{\partial\Psi_m}{\partial\beta_d}+\frac{\partial\Phi_m}{\partial\dot{\beta}_d} = c_d\dot{\beta}_d + \Psi_m^{ID} - w_d + \partial\mathrm{I}_{[0,1]}\left(\beta_d\right), \tag{24a}$$

$$\begin{aligned}\frac{b_2}{n_a} \in \frac{1}{\ell_{m,o}}\left[\frac{\partial\mathcal{E}_w}{\partial\beta_w}+\frac{\partial\mathcal{D}_w}{\partial\dot{\beta}_w}\right] = \frac{1}{\ell_{m,o}}\Big[c_w\dot{\beta}_w+\mathcal{E}_w^{sp}-w_w+\\ +\partial\mathrm{I}_{[0,1]}\left(\beta_w\right)+\partial\mathrm{I}^+(\dot{\beta}_w+\bar{\beta}_w^{\omega}v_w)\Big],\end{aligned} \tag{24b}$$

$$\begin{aligned}\frac{b_3}{\mathcal{A}_c} \in \frac{\partial\Psi_m}{\partial\beta_m}+\frac{\partial\Phi_m}{\partial\dot{\beta}_m} = c_m\dot{\beta}_m+\Psi_m^b-w_m+\partial\mathrm{I}_{[0,1]}(\beta_m)+\\ +\partial\mathrm{I}_{[-v_m,0]}(\dot{\beta}_m),\end{aligned} \tag{24c}$$

$$h_1 = k_1\beta_{1/3}, \quad h_2 = k_2\beta_{2/3}, \quad h_3 = k_3\beta_{3/3}. \tag{24d}$$

Accordingly, governing equations of fibril's elasto-damage behavior are obtained by combining equilibrium conditions (5) with interscale compatibility relationships (17), (18), and (20) and constitutive relationships (23) and (24).

For evaluating model performance, MDS/experimental data on homogenous uniaxial traction only are available in

literature. Accordingly, in the present work, equilibrium relationships are solved by considering $F_f \neq 0$ and $q_f = a_f = 0$ in order to reproduce numerical/experimental conditions.

In this simplifying case, equilibrium Eq. (5a) with boundary conditions (5c) reduces to

$$\sigma_f = \frac{F_f}{\mathcal{A}_f} = \rho_a \sigma_m = \rho_a \left(\sigma_w + \sigma_c\right), \tag{25}$$

where $\rho_a = \mathcal{A}_c/\mathcal{A}_f$ is the ratio between load-bearing area and total fibril cross-sectional area, σ_f is fibril nominal stress related to molecular stress $\sigma_m = \sigma_m(\varepsilon_m^e)$ [see Eq. (14)], weak cross-links stress $\sigma_w = k_w \delta_w^e/\mathcal{A}_m$, and covalent cross-links stress $\sigma_c = \lambda_c^D \sigma_c^D + \lambda_c^T \sigma_c^T$ where $\sigma_c^D = k_c^D \delta_c/\mathcal{A}_m$ and $\sigma_c^T = k_c^T \delta_c/\mathcal{A}_m$ refer to immature divalent and mature trivalent cross-links, respectively.

Governing equation for fibril stretch is obtained by combining Eqs. (17), (18), (23), and (25), and it results

$$\begin{aligned}\bar{\sigma}_m + \bar{E}_m \bar{\beta}_3 \left[\nu_1 \frac{\bar{\ell}_R}{\ell_{m,o}} de_1 - \alpha_1 \frac{\bar{\varepsilon}_m^e d\tau}{\tau_o^{ID}}\right] - \bar{E}_m \alpha_3 \frac{\bar{\varepsilon}_m^e d\tau}{\tau_o^{MR}} = \\ = \frac{1}{\mathcal{A}_m}\left[\bar{r}_c + k_c^{eq} \bar{\ell}_R f_c\left(\bar{\delta}\right) de_2 + \bar{r}_w^e + k_w \nu_2 \bar{\ell}_R de_2\right],\end{aligned} \tag{26}$$

where $\bar{r}_c = k_c^{eq} \bar{\delta}_c$ and $\bar{r}_w^e = k_w \bar{\delta}_w^e$.

Moreover, let introduce

$$d\check{\beta}_1 := \frac{d\tau}{c_d}\left(w_d - \frac{H_0\left(\lambda_c^T\right)\mathcal{E}_c^T\left(\tilde{\varepsilon}_c\right) + H_0\left(\lambda_c^D\right)\mathcal{E}_c^D\left(\tilde{\varepsilon}_c\right)}{\Omega_{m,o}}\right), \tag{27a}$$

$$d\check{\beta}_2 := \max\left\{\frac{d\tau}{c_w}\left(w_w - \mathcal{E}_w^{el}\left(\tilde{\varepsilon}_w^e\right)\right), -\bar{\beta}_w^{\omega} v_w d\tau\right\}, \tag{27b}$$

$$d\check{\beta}_3 := \max\left\{\min\left\{\frac{d\tau}{c_m}\left(w_m - \Psi_m^e\left(\tilde{\varepsilon}_m^e\right)\right), 0\right\}, -v_m d\tau\right\}. \tag{27c}$$

It is worth pointing out that, from previous relationships, the quantity $d\check{\beta}_2/d\tau + \bar{\beta}_w^{\omega} v_w \geq 0$ is *a priori* in the definition domain of $\partial \mathrm{I}^+$. Similarly, $-v_w \leq d\check{\beta}_3/d\tau \leq 0$, and thereby, the quantity $d\check{\beta}_3/d\tau$ is *a priori* in the definition domain of $\partial \mathrm{I}_{[-v_m,0]}$. Accordingly, by denoting $\check{\beta}_j = \bar{\beta}_j + d\check{\beta}_j$ and from the definition domain of $\partial \mathrm{I}_{[0,1]}$, damage parameters β_j are obtained from

$$\beta_j = \begin{cases} \check{\beta}_j & \text{if } \check{\beta}_j \in [0,1] \\ \bar{\beta}_j & \text{else} \end{cases}, \tag{27d}$$

being solutions for Eq. (5b), combined with Eqs. (20) and (24). It is worth pointing out that, under homogenous uniaxial traction, $\beta_{1/3} = \beta_{2/3} = \beta_{3/3} = 0$ for any $\xi_3 \in [0, \ell_f]$, because all quantities are constant in space. Accordingly, results are not affected by damage diffusion coefficients k_j.

In Eq. (27), the onset of damage is governed by damage thresholds w_w, w_d, and w_m. Useful relationships for setting the values of the latter starting from available data are:

$$w_w = \frac{K_w \varepsilon_{SP}^2}{2}, \quad \sigma_{SP} = \frac{K_w \varepsilon_{SP}}{\mathcal{A}_m \ell_{m,o}}, \quad \sigma_{SP} = \frac{\sigma_f^{SP}}{\rho_a} \tag{28a}$$

$$w_d = \frac{K_{ID} \varepsilon_{ID}^2}{2\Omega_{m,o}}, \quad \sigma_{ID} = \frac{K_{ID} \varepsilon_{ID}}{\mathcal{A}_m \ell_{m,o}}, \quad \sigma_{ID} = \frac{\sigma_f^{ID}}{\rho_a} \tag{28b}$$

$$w_m = \Psi_m^e(\varepsilon_{MR}), \quad \text{with } \varepsilon_{MR} \text{ such that:}$$

$$\sigma_m(\varepsilon_{MR}) = \sigma_{MR} = \frac{\sigma_f^{MR}}{\rho_a}, \tag{28c}$$

with $K_{ID} = H_0(\lambda_c^T) K_c^T + H_0(\lambda_c^D) K_c^D$ and where, referring to the onset of SP, ID and MR, ε_* and σ_* are the strain (normalized with respect to $\ell_{m,o}$) and the stress (normalized with respect to $\mathcal{A}_m$) at constituent scale, while σ_f^* is the stress (normalized with respect to $\mathcal{A}_f$) at fibril scale (with $* = \{SP,\ ID,\ MR\}$). In other words, introducing the ID-related covalent cross-link-stress

$$\sigma_c^{ID} := H_0\left(\lambda_c^D\right)\sigma_c^D + H_0\left(\lambda_c^T\right)\sigma_c^T, \tag{29}$$

a damage mechanism activates when the corresponding stress reaches its threshold value: when $\sigma_w = \sigma_{SP}$, then SP activates; when $\sigma_c^{ID} = \sigma_{ID}$, then ID activates; when $\sigma_m = \sigma_{MR}$, then MR activates.

3 Results

The outcomes obtained by proposed model are compared with both results from atomistic computations and experimental data on fibril monotonic uniaxial traction. Moreover, an application reproducing a traction loading–unloading test is proposed.

In a displacement-based approach where fibril nominal strain $\varepsilon_f := u/\ell_{f,o}$ is the control variable, Eqs. (26) and (27) can be solved in the variables de_k and β_j by accounting for the compatibility incremental relationship:

$$d\varepsilon_f = d\varepsilon_R = d\varepsilon_m + d\varepsilon_{CL} = \frac{\left(de_1 + de_2\right)\bar{\ell}_r}{\ell_{m,o}} = \dot{\ell}_f \frac{d\tau}{\ell_{f,o}}. \tag{30}$$

The influence on fibril mechanics of the values of

- cross-link densities λ_c^D and λ_c^T,
- parameters ω, c_w/w_w and v_w,
- molecular relaxation time constant τ_o^{MR},

is shown in order to discuss on their sensitivity and to justify modeling choices. Parametric analyses for other model parameters are herein not addressed because they are already discussed in previous works (Maceri et al. 2012b; Marino and Vairo 2014a).

Results will be shown in terms of fibril constitutive relationship σ_f versus ε_f and the evolution of damage variables β_j. Moreover, internal state variables $\mathcal{S}_R$ and stresses σ_m [see Eq. (14)], σ_c, σ_c^{ID} and σ_w [see Eqs. (25) and (29)] are reported. Furthermore, the tangent modulus related to the fibril (E_f), to the weak cross-links (E_w) and to the covalent cross-links (E_c),

$$E_f := \frac{\partial \sigma_f}{\partial \varepsilon_f}, \quad E_w := \frac{\partial \sigma_w}{\partial \varepsilon_{CL}}, \quad E_c := \frac{\partial \sigma_c}{\partial \varepsilon_{CL}}, \tag{31}$$

will be shown, obtaining also the overall intermolecular stiffness $E_{CL} = E_c + E_w$, through the consideration that weak and covalent cross-links are *in-parallel* mechanisms. By referring to Eq. (15), molecular stiffness $E_m(\varepsilon_m(\bar{\varepsilon}_f))$ will be reported together with entropic $E_m^s(\varepsilon_m^{e,s}(\bar{\varepsilon}_f))$ and energetic $E_m^h(\varepsilon_m^{e,h}(\bar{\varepsilon}_f))$ contributions. Finally, the values at fibril failure (assumed to occur when fibril stress starts to decrease with increasing strain) for σ_c^{ID}, σ_m, σ_f, ε_c, ε_m^e and ε_f will be denoted as s_c^{ID}, s_m, s_f, d_c, d_m^e and d_f, respectively.

As a result of a sensitivity analysis, computational steps have been chosen in order to obtain strain increments $d\varepsilon_f$ such that $\varepsilon_f^{end} = 2 \cdot 10^4 |d\varepsilon_f|$ where ε_f^{end} is the fibril strain at the end of the simulation ($\varepsilon_f^{end} = 0.5$ for MDS and $\varepsilon_f^{end} = 0.26$ for experiments). All simulations are performed at the body temperature $T = 310\,\mathrm{K}$, employing $\rho_a = \mathcal{A}_c/\mathcal{A}_f = 0.7$ from experimental data (Holmes et al. 2001; Marino and Vairo 2014a).

3.1 Comparison with MDS data

Model predictions are compared with results obtained by means of MDS approaches (Buehler 2008) where the uniaxial traction (with displacement rate $\dot{\ell}_f = 0.4$ m/s) of an array of 2×5 collagen molecules is considered ($n_a = 5$, $n_s = 2$, $\ell_c = 287\,\mathrm{nm}$, and $\mathcal{A}_m = 1.41\,\mathrm{nm}^2$).

MDSs have been carried out by Buehler (2008) adopting coarse-grained models of collagen fibrils and employing some simplifying assumptions. The latter can be straightforwardly reproduced by the proposed model, and in order to have a meaningful comparison, values of model parameters are chosen in order to reproduce the atomistic numerical model adopted in Buehler's simulations. The procedure adopted for setting the values of model parameters is explained in what follows.

Buehler includes weak cross-links through a Lennard-Jones potential, and covalent cross-links are modeled through an increased Lennard-Jones adhesion at the ends of each molecule where a constant proportionality factor of $\varpi = 12.5$ corresponds to one covalent cross-link for each molecule and $\varpi = 1$ to zero covalent cross-links for each molecule. Since Buehler's model is bidimensional, immature divalent cross-links are considered only. Accordingly, cross-link density parameters are computed as $\lambda_c^D = (\varpi - 1)/11.5$, $k_w = k_c^D/11.5$, $\lambda_c^T = 0$, and k_c^T is ineffective.

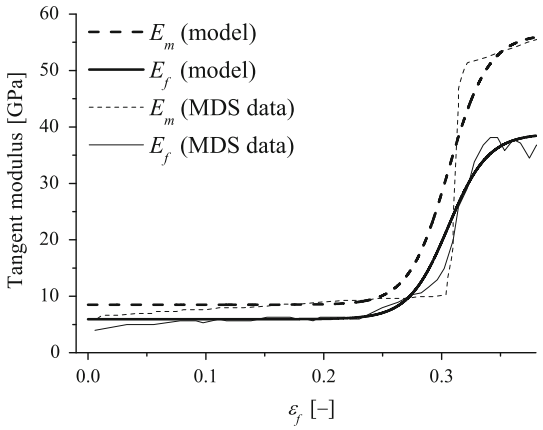

Fig. 4 Multiscale analytical model applied to coarse-grained atomistic conditions. Fibril E_f and molecular E_m tangent moduli versus fibril strain ε_f. Comparison between present model and molecular dynamics simulations (MDSs) by Buehler (2008) employing the increased adhesion proportionality factor $\varpi = 25$, (namely, $\lambda_c^D = (\varpi - 1)/11.5 \approx 2$). The values of model parameters are reported in text (see Sect. 3.1)

Moreover, the delayed activation of covalent cross-links is not considered in Buehler's simulations. This is reproduced by employing $f_c(x) = 1$, instead of the expression given in Eq. (8b), in the interscale compatibility relationships. Furthermore, addressing collagen elasticity, Buehler neglects entropic mechanisms. Thereby, it is chosen $\ell_{m,o} \to \ell_c$ in order to obtain $E_m^s \to +\infty$ [see Eq. (15c)] and $E_m \to E_m^h$ [see Eq. (15a)].

For setting the remaining parameters governing fibril response in the purely elastic regime $\beta_1 = \beta_2 = \beta_3 = 1$ [that is, parameters in Eq. (15d), and k_c^D], Buehler's data on functions $E_m(\varepsilon_f)$ and $E_f(\varepsilon_f)$, available for $\varpi = 25$, have been fitted by means of a trial-error procedure. Accordingly, as shown in Fig. 4 and by choosing $\hat{E}_o = 8.5\,\mathrm{GPa}$, $\hat{E} = 48\,\mathrm{GPa}$, $\eta = 60$, $\varepsilon_o^h = 0.305$, and $k_c^D = 7\,\mathrm{nN/nm}$, the good agreement between obtained and available data for both $E_m(\varepsilon_f)$ and $E_f(\varepsilon_f)$ at $\varpi = 25$ proves the correspondence between Buehler's and the proposed model for what concerns fibril elastic response.

Addressing damage-related parameters in Eq. (27), their values are set by means of the following considerations:

– damage thresholds w_w, w_d and w_m are set on the basis of fibril strengths by means of Eq. (28). By referring to a given value of the increased adhesion proportionality factor ϖ, s^{ϖ} denotes the ultimate stress value obtained by Buehler's simulations, and it is chosen

$$\sigma_f^{SP} = s^1, \quad \sigma_f^{ID} = \frac{s^5 + s^{10} + s^{15} + s^{20} + s^{25}}{5},$$
$$\sigma_f^{MR} = \frac{s^{35} + s^{40}}{2},$$

because: $\varpi = 1$ corresponds to zero covalent cross-links and thereby to the activation of SP; $\varpi = 5, 10, 15, 20$ and 25 are associated with softening-yielding behavior, herein associated with ID; $\varpi = 35$ and 40 correspond to fibril brittle rupture, related to MR. Accordingly, it results $\sigma_f^{SP} = 0.38\,\text{GPa}$, $\sigma_f^{ID} = 2.29\,\text{GPa}$, and $\sigma_f^{MR} = 6.29\,\text{GPa}$.

- damage rate is governed by the normalized damage viscosity parameters c_*/w_* (with $* = \{w, d, m\}$) and, for SP and MR, maximum damage rates v_w and v_m. In agreement with the non-smoothness of Buehler's data, a quasi-instantaneous damage is herein assumed by choosing $c_*/w_* = 1/v_w = 1/v_m = 1\,\text{ps}$;
- molecular relaxation time constant associated with ID is chosen by fitting the stress softening-rate for $\varpi = 10$ and its results equal to $\tau_o^{ID} = 0.6\,\mu\text{s}$; molecular relaxation time constant associated with MR is chosen from the slope of the stress drop obtained at fibril failure for $\varpi = 35$ and it results $\tau_o^{MR} = 10\,\text{ns}$.

Addressing different values of covalent cross-link density, the comparison between obtained constitutive relationship and available MDS data is shown in Fig. 5. Addressing the entire range of values for cross-link density, the average error on fibril ultimate stress results to be equal to 3.9 %. Moreover, Fig. 6 shows the evolution of damage variables β_j as well as of nanoscale strain measures associated with the dominant mechanisms that govern fibril mechanics.

3.2 Comparison with experimental data

Model predictions are compared with experimental data by Svensson et al. (2013) on the uniaxial traction of long collagen fibrils at constant elongation rate, $\dot{\ell}_f = 40\,\mu\text{m/s}$. Collagen fibrils from both human-patellar tendon (HPT, length $\ell_{f,o} = 33.05\,\mu\text{m}$ and diameter $2r_f = 0.153\,\mu\text{m}$) and rat-tail tendon (RTT, length $\ell_{f,o} = 29.50\,\mu\text{m}$ and diameter $2r_f = 0.190\,\mu\text{m}$) are addressed.

The values of model parameters employed in the present application are listed in Table 1. Biophysical parameters governing molecular elastic response are chosen on the basis of well-established results (Buehler and Wong 2007; Maceri et al. 2012b; Marino and Vairo 2013, 2014c). The density of mature cross-links is the one reported from biochemical analysis by Svensson et al. (2013), while immature cross-link density is chosen on the basis of experimental studies by Saito et al. (1997). Other model parameters are tuned in order to fit the available experimental data by following a trial-error procedure. A unique set of parameters governing the elasto-damage response of collagen molecules and of covalent cross-links (except for their density) are employed for HPT and RTT fibrils, while parameters governing the intermolecular weak interactions are kept independent for the two cases herein addressed.

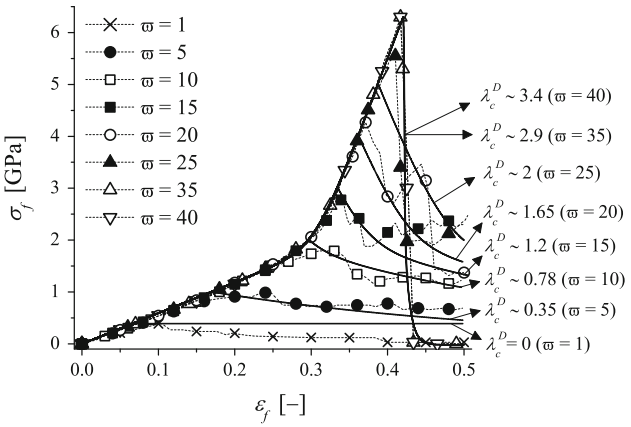

Fig. 5 Multiscale analytical model applied to coarse-grained atomistic conditions. Stress σ_f versus strain ε_f constitutive relationship of a collagen fibril with varying cross-link density λ_c^D: comparison between predictions obtained by means of proposed model (*continuous lines*) and of molecular dynamics simulations (*dashed lines* with *symbols*) by Buehler (2008). Different values of Buehler's increased adhesion proportionality factor ϖ, with $\lambda_c^D = (\varpi - 1)/11.5$, are addressed. The values of model parameters are reported in text (see Sect. 3.1)

The comparisons between experimental data and model outcomes are presented in Fig. 7 in terms of both E_f versus ε_f and σ_f versus ε_f relationships. Choosing experimental data as a reference, it is obtained an average error of about 1 % for the σ_f versus ε_f curves on the overall strain range. Moreover, an average error of 5 % on the E_f versus ε_f curves within $\varepsilon_f \in [0, 0.19]$ for HPT and $\varepsilon_f \in [0, 0.15]$ for RTT fibrils (namely, before fibril failure) is reported. Error estimates are obtained normalizing with respect to the maximum experimental stress and tangent modulus, respectively, for the case under investigation.

The evolution of RUS state variables (both strain and damage variables) and internal stresses are reported in Fig. 8 where strong nonlinearities clearly appear and couple each other. Addressing the HPT case, stiffness nonlinearities of fibril constituents are shown in Fig. 9 and compared with the overall fibril stiffness, in order to highlight the mechanisms which governs fibril behavior at different strain-range values. Moreover, Fig. 9 shows also the dependence on cross-link density of stresses and strains (both for constituent and for the overall fibril) at failure. This allows to highlight the dependence of fibril mechanical response on cross-link biochemistry.

Finally, Fig. 10 presents a parametric analysis on the values of parameters governing the weak cross-link damage law

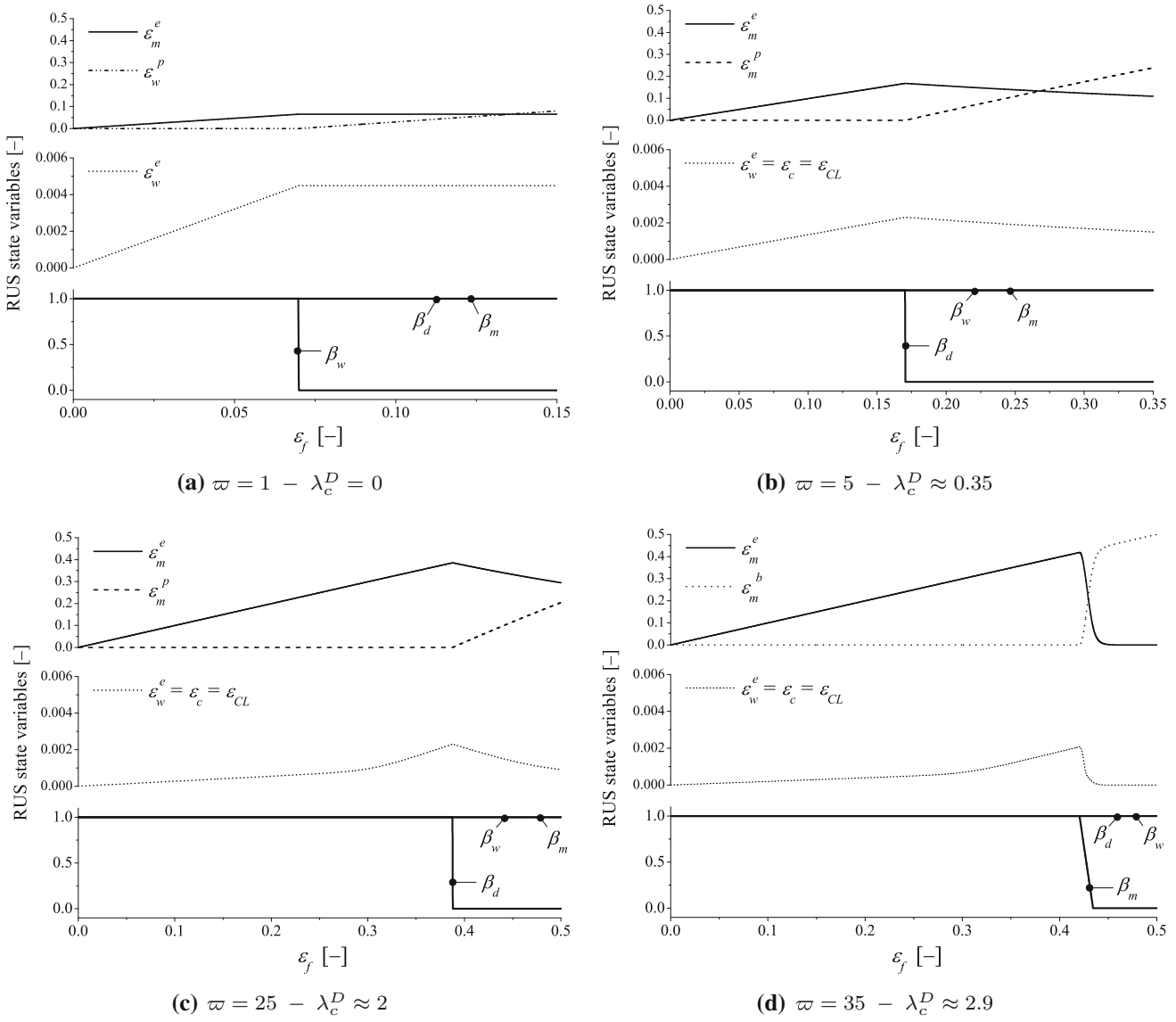

(a) $\varpi = 1 \;-\; \lambda_c^D = 0$ **(b)** $\varpi = 5 \;-\; \lambda_c^D \approx 0.35$

(c) $\varpi = 25 \;-\; \lambda_c^D \approx 2$ **(d)** $\varpi = 35 \;-\; \lambda_c^D \approx 2.9$

Fig. 6 Multiscale analytical model applied to coarse-grained atomistic conditions. State variables in a fibril representative unit system (RUS) versus fibril strain ε_f with different values of Buehler's increased adhesion proportionality factor ϖ, namely with varying cross-link density $\lambda_c^D = (\varpi - 1)/11.5$. The values of model parameters are reported in text (see Sect. 3.1)

and molecular relaxation time constant following the activation of MR.

3.3 Application: loading–unloading behavior

Three cycles of a traction loading–unloading displacement-driven test at constant elongation rate $|\dot{\ell}_f| = 40\,\mu$m/s are addressed. The values employed for model parameters coincide with the ones of the HPT case. Accordingly, $\ell_{f,o} = 33.05\,\mu$m, $2r_f = 0.190\,\mu$m and other model parameters are listed in Table 1. Figure 11 shows the applied strain-law $\varepsilon_f(\tau)$ and the underlying deformation mechanisms occurring at nanoscale. Moreover, the evolution of damage variables is reported together with the fibril stress normalized with respect to σ_f^{MR}. As a result of nanoscale mechanisms, fibril constitutive response (reported in the same figure) is characterized by hysteresis loops associated with SP (namely, β_w) up to final failure due to MR (namely, β_m).

4 Discussions

Present paper addresses collagen fibril mechanics with a special insight on elasto-damage mechanisms occurring at nanoscale. The role of cross-links on determining the well-established variability in fibril mechanical response is clearly highlighted through a multiscale modeling approach.

Table 1 Values of model parameters employed for comparison with experimental data by Svensson et al. (2013) for fibrils in human-patellar tendon (HPT) and rat-tail tendon (RTT)

MOLECULAR RESPONSE
(the same for HPT and RTT)

	$\ell_{m,o}$	ℓ_c	ℓ_p	$\mathcal{A}_m$	$\hat{E}_o$	$\hat{E}$	η	ε_o^h
Elastic[a]:	nm	nm	nm	nm^2	GPa	GPa	–	–
	279	287	14.5	1.41	1	80	22.5	0.1

	w_m	v_m	$\frac{c_m}{w_m}$	τ_o^{MR}	w_d	$\frac{c_d}{w_d}$	τ_o^{ID}
Damage:	$\frac{\text{pN}}{\text{nm}^2}$	s^{-1}	ns	ms	$\frac{\text{pN}}{\text{nm}^2}$	μs	ms
	17	25	1	0.1	4.2	10	1.1

INTERMOLECULAR RESPONSE

	λ_c^T	λ_c^D	k_c^T	k_c^D	μ	δ_o	k_w	ω	w_w	v_w	$\frac{c_w}{w_w}$
	mmol/mol	mmol/mol	$\frac{\text{nN}}{\mu\text{m}}$	$\frac{\text{nN}}{\mu\text{m}}$	–	nm	$\frac{\text{nN}}{\mu\text{m}}$	–	nN·nm	s^{-1}	μs
HPT	890[b]	1400[c]	105	5	0.08	35	75	0.55	0.05	27	10
RTT	8.7[b]						50	0.45	0.06		

[a] In agreement with Buehler and Wong (2007), Maceri et al. (2012b), Marino and Vairo (2013, 2014c)
[b] From Svensson et al. (2013); [c] from Saito et al. (1997)

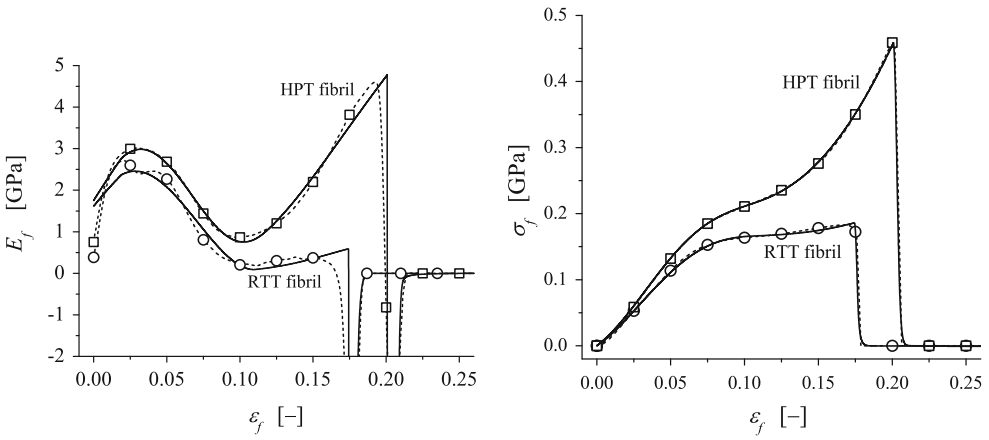

Fig. 7 Comparison between experimental data (*dashed lines* with *symbols*) by Svensson et al. (2013) and predictions obtained by means of proposed model for collagen fibrils in human-patellar tendon (HPT) and rat-tail tendon (RTT). *Left* Fibril tangent modulus E_f versus strain ε_f. *Right* Fibril stress σ_f versus strain ε_f constitutive relationship. The values of model parameters are reported in Table 1

• *Reproduction of MDS data*

The comparison with MDS data by Buehler (2008) clearly shows that model predictions agree well with coarse-grained atomistic computations of short fibrils (see Fig. 5). In fact, several features of available data are reproduced: for low cross-link density, fibril strength increases with cross-link density and damage behavior shows large yielding regimes; for high covalent cross-link density, fibril damage behavior is characterized by a brittle-like rupture and the overall mechanical response has very low sensitiveness to cross-link density. Moreover, the nanoscale mechanisms governing the response in the different cases addressed by Buehler can be straightforwardly analyzed thanks to the proposed multiscale analytical technique (see Fig. 6). When only weak interactions among molecules are present, SP activates (associated with β_2) and fibril behavior is mainly governed by molecular elastic deformation ε_m^e in the elastic regime and by permanent molecular slippage ε_w^p in the yielding regime; with increasing covalent cross-link density, ID occurs at fibril failure (associated with β_1 and ε_m^p); when the density of covalent cross-links is high, fibril damage is due to the rupture of covalent bonds inside collagen triple-helix structure (namely, activation of β_3 and ε_m^b) and there is the transition from a yielding to a brittle behavior.

It is worth to point out the good quantitative agreement between obtained results and available data for the entire range of values considered for covalent cross-link density. Clearly, with respect to MDS, the proposed analytical technique reduces significantly the computational costs, resulting in the order of a minute for each simulation on a laptop with 2.3 GHz Quad-core Intel i7 processor.

With reference to the yielding behavior for cross-links deficient-fibrils, obtained results agree well with the initial softening-rate obtained by Buehler's coarse-grained data.

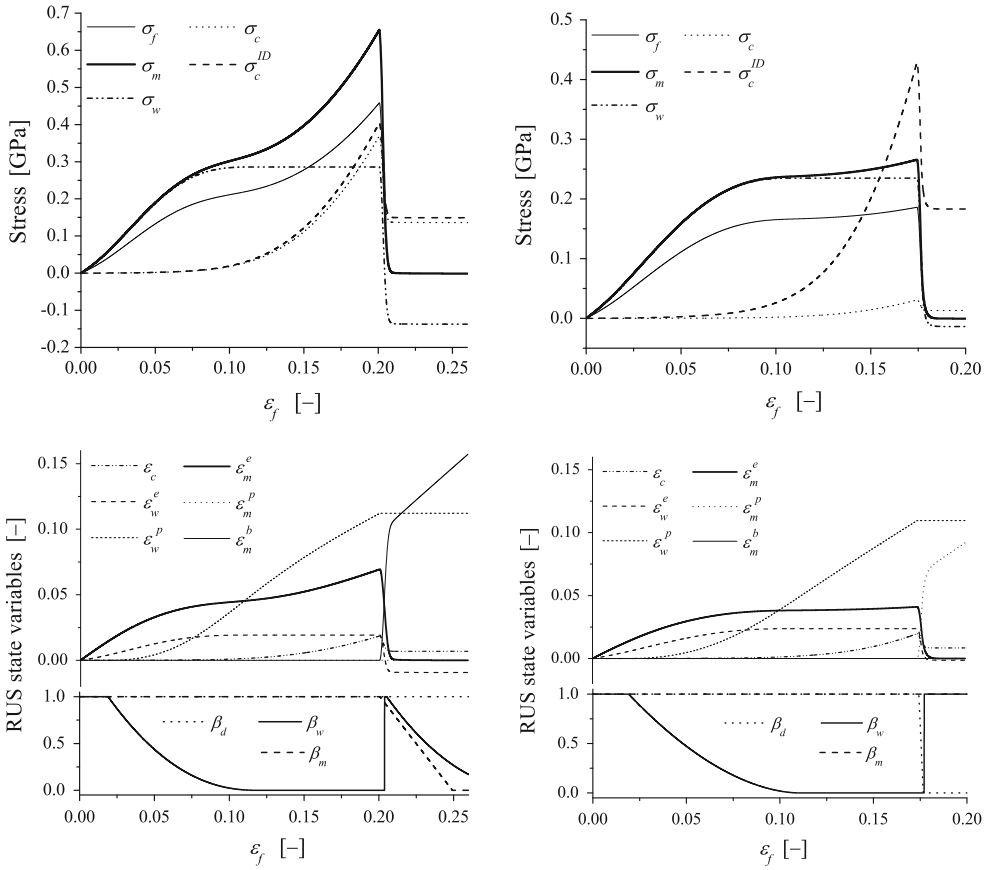

Fig. 8 Stresses (*top*) and state variables (*bottom*) in a representative unit system (RUS) of fibrils in human-patellar (*left*) and rat-tail (*right*) tendons versus fibril strain ε_f. It is worth pointing out that $\varepsilon_m^p = 0$ (resp., $\varepsilon_m^b = 0$) during the overall test for human-patellar (resp., rat-tail) fibrils, and thereby the curve is not clearly visible. The values of model parameters are reported in Table 1

Nevertheless, it is worth remarking that, for $\varpi = 1$ (namely, $\lambda_c^D = 0$), proposed model predicts a perfectly yielding behavior without softening (due to SP onset), in contrast to available data. The choice of not including softening for SP is based on non-coarse-grained MDS results on the assembly of two tropocollagen segments (Buehler 2006; Uzel and Buehler 2011; Marino and Vairo 2014a). Nevertheless, different yielding behaviors for SP could be addressed by modifying only weak cross-links interscale compatibility relationships [namely, Eq. (18)] and by introducing a possible molecular relaxation (similar to ID and MR).

Despite MDSs allow to have an insight on fibril elasto-damage internal mechanisms, attention should be paid when quantitative predictions are addressed. For instance, the highest value of fibril stiffness predicted from the coarse-grained MDSs by Buehler (≈40 GPa, see Fig. 4) is indeed higher than the one obtained from experimental data from well-established literature (in the range ≈1–10 GPa, Cusack and Miller 1979; Shen et al. 2008; Svensson et al. 2013). This occurrence is due to entropic effects and large-strain rates, (Buehler 2008). Accordingly, a comparison between model and experimental results is necessary for proving model capabilities in providing quantitative predictions.

• *Reproduction of experimental data*

Model results have been also compared with experimental data by Svensson et al. (2013), revealing model capability in reproducing the mechanics of collagen fibrils in both human-patellar and rat-tail tendons. Model fits available data in an excellent way for both specimen types (see Fig. 7). Available biochemical data on the values of cross-link density (Saito et al. 1997; Svensson et al. 2013), are straightly incorporated in the simulations thanks to the multiscale approach within which present model is developed.

Molecular biophysical properties are chosen the same among HPT and RTT cases because collagen polypeptide pattern does not differ among different species and genetic disorders are herein not addressed. Similarly, a unique set for covalent cross-link properties is chosen, except from the density of mature cross-links. On the other hand, differences in the biochemical environment of different specimens (and especially fibrils from human-patella and rat-tails) justify the

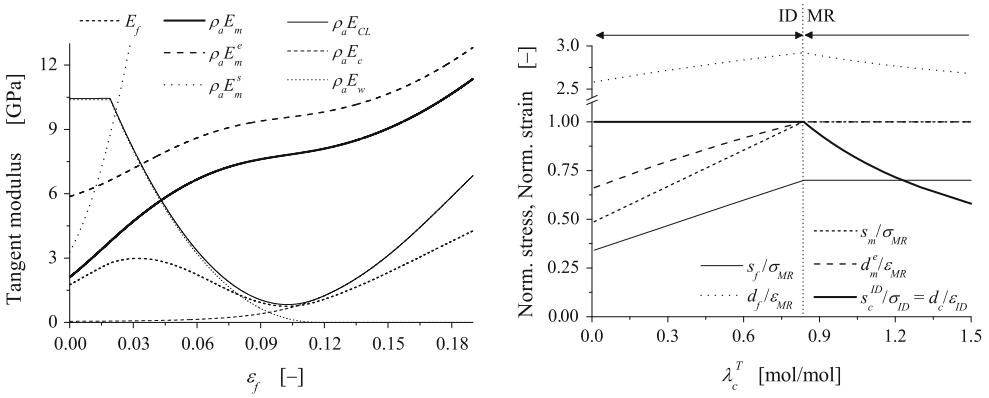

Fig. 9 Analysis of internal stiffness and damage mechanisms. *Left* Fibril (E_f), molecular (E_m, E_m^e and E_m^s), and intermolecular (E_{CL}, E_c and E_w) tangent moduli versus fibril strain ε_f. Stiffness of internal constituents are scaled with the load-bearing-to-total area ratio $\rho_a = \mathcal{A}_c/\mathcal{A}_f$. *Right* Normalized stress and strain at failure versus λ_c^T for: covalent cross-links (s_c^{ID}/σ_{ID} and d_c/ε_{ID}); molecules (s_m/σ_{MR} and d_m^e/ε_{MR}); fibril (s_f/σ_{MR} and d_f/ε_{MR}). If not differently specified, the values of model parameters are reported in Table 1 and refer to fibrils in human-patellar tendon. By employing Eq. (28), values of damage thresholds correspond to $\sigma_{ID} = 427.6\,\text{MPa}$, $\varepsilon_{ID} = 1.96\,\%$, $\sigma_{MR} = 654.6\,\text{MPa}$, $\varepsilon_{MR} = 6.94\,\%$

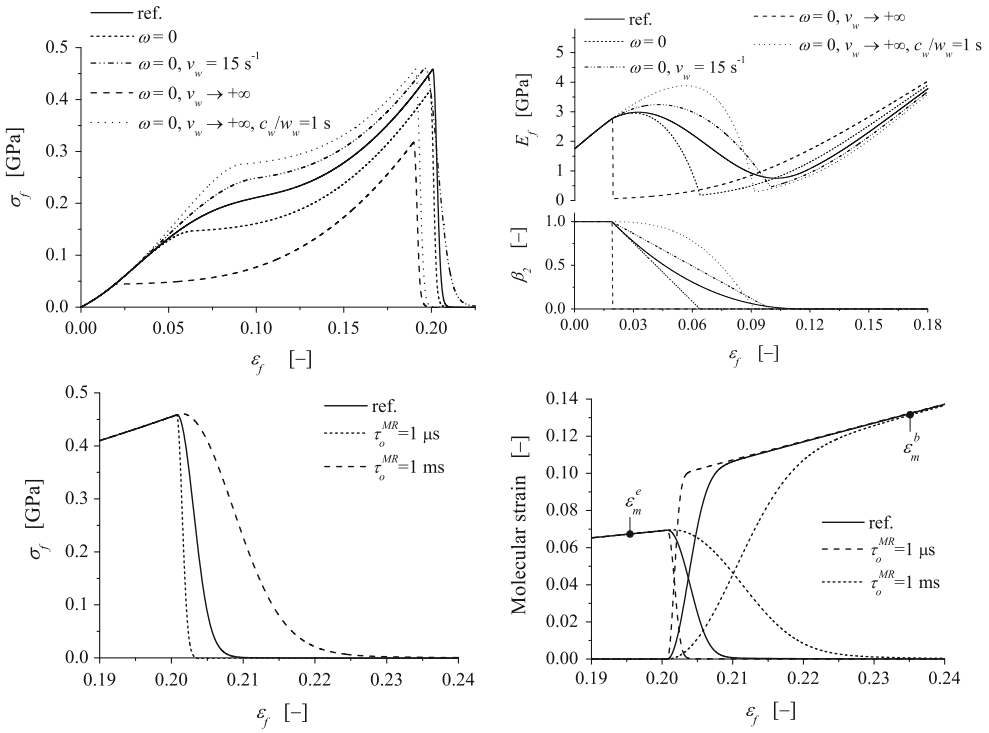

Fig. 10 Parametric analyses on values of model parameters. *Top* Fibril stress σ_f (*left*), tangent modulus E_f and damage variable β_2 (*right*) versus strain ε_f for different values of parameters governing weak cross-links damage laws. *Bottom* Fibril stress σ_f (*left*), elastic ε_m^e and MR-inelastic ε_m^b molecular strains (*right*) versus strain ε_f for different values of τ_o^{MR}. If not differently specified, the values of model parameters are reported in Table 1 and refer to fibrils in human-patellar tendon

choice of allowing for different intermolecular weak interaction behaviors (Grant et al. 2009; Gautieri et al. 2012). Accordingly, model parameters governing weak cross-links properties are set independently for HPT and RTT fibrils. Nevertheless, as a further proof of consistency, the best fitting is obtained employing values of model parameters with the same order of magnitude among the two cases, and sometimes their values coincide.

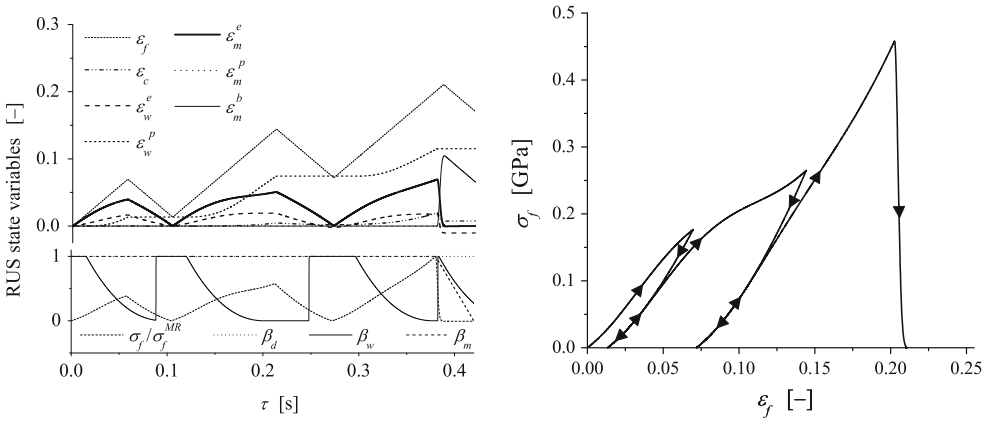

Fig. 11 Three loading–unloading cycles of a displacement-driven traction test at $|\dot{\ell}_f| = 40\,\mu$m/s. *Left* Evolution of applied fibril strain ε_f, nanoscale strains ε_c, ε_w^e, ε_w^p, ε_m^e, ε_m^p,and ε_m^b, normalized fibril stress σ_f/σ_f^{MR}, and damage variables β_d, β_w and β_m versus time τ. It is worth pointing out that $\varepsilon_m^p = 0$ during the overall test, and thereby the curve is not clearly visible. *Right* Fibril stress σ_f versus strain ε_f. The values of model parameters are reported in Table 1 and refer to fibrils in human-patellar tendon ($\ell_{f,o} = 33.05\,\mu$m and $2r_f = 0.190\,\mu$m)

– Analysis of fibril mechanics

The model allows to predict and to put in evidence the high nonlinearities occurring in the internal structure of HPT and RTT fibrils (see Fig. 8). Moreover, the analysis of constituent's stiffness is useful for determining the mechanisms which mainly affect fibril response (see Fig. 9). When *in-series* mechanisms are considered, the one associated with a lower stiffness dominates fibril behavior. On the other hand, addressing *in-parallel* mechanisms, the stiffer one is the most important. From this point of view, fibril mechanics can be described as the result of the complex interplay of a number of nonlinear stiffnesses: some of them are *in-series* (namely, molecular E_m and intermolecular E_{CL} but also entropic E_m^s and energetic E_m^h) and others *in-parallel* (covalent E_c and weak E_w cross-links).

For strains in the range $\varepsilon_f \in [0, 0.02]$, fibril mechanics is governed by both molecular elastic deformation ε_m^e and reversible molecular sliding associated with weak cross-links deformation δ_w^e. Moreover, average molecular strain ε_m within this interval is 1.61 % for HPT and 1.47 % for RTT while sliding mechanisms contribute to the overall fibril deformation for the remaining part (that is, 0.39 % for HPT and 0.53 % for RTT). This agrees in an excellent way with X-ray diffraction studies by Sasaki and Odajima (1996) who, in 2 % of overall strain, report a contribution from molecular elongation equal to 1.7 % and from molecular rearrangement mechanisms equal to 0.3 % for fibrils in Achilles tendon. This evidence is a strong proof for the effectiveness of the proposed approach since it highlights model capability in capturing *a-posteriori* a main experimental observation on nanostructural intra-fibril rearrangement during tensile loads in tendons. Thereby, in this low-strain range, fibril mechanics is mainly affected by molecular deformation, as also confirmed by the evidence that $E_m << E_{CL}$. Moreover $E_{CL} \approx E_w$ because the covalent cross-link is not yet activated ($E_c \approx 0$). Furthermore, it is worth highlighting that entropic mechanisms (namely, thermal fluctuations) have a strong influence on the overall molecular behavior and, since $E_m^s < E_m^h$, they significantly reduce molecular modulus with respect to the value obtained if only energetic mechanisms were considered. This justifies the need of incorporating the complex and refined molecular behavior herein addressed [see Eq. (15)].

For $\varepsilon_f \in [0.02, 0.1]$, fibril deformation is mainly related to SP activation ($E_{CL} \approx E_w << E_m$). The load reaches the bond strength of weak intermolecular cross-links and the irreversible sliding between collagen molecules occurs at the expense of the elastic one and of molecular deformation (namely, ε_w^p increases, ε_w^e and ε_m tend to remain constant). Clearly, SP is associated with a significant reduction in fibril stiffness.

For $\varepsilon_f > 0.1$, fibril stiffness increases again up to the final failure because of the activation of intermolecular covalent cross-links ($E_{CL} \approx E_c >> E_w$). This delayed response is related to the straightening of the hook-shaped telopeptide in which covalent cross-links form, herein modeled through Eq. (8b), (Marino and Vairo 2014a). The stiffening effect is significant for HPT and negligible for RTT, suggesting that it is mainly due to the presence of mature trivalent cross-links which are responsible for transverse connections between different microfibrils (Bailey et al. 1998; Orgel et al. 2006; Yang et al. 2012), and in fact it results $k_c^T >> k_c^D$.

– Biochemistry-dependent fibril failure

Fibril failure behavior is significantly affected by the density of mature cross-links. In fact, HPT failure is due to the activation of damage parameter β_3 associated with MR-

inelastic strain ε_m^b. On the other hand, RTT failure is related to the activation of β_1 associated with ID-inelastic strain ε_m^p. The reason underlying the transition from ID to MR is well highlighted by means of present model and by taking into account that the onset of ID is associated to the force transmitted through the covalent cross-links, representing a pulling out force for the polypeptide strand where the covalent cross-link is formed. The latter force has to be not confused with the one that intervenes in fibril equilibrium (25), namely σ_c, which is an homogenous stress measure representing the average force transmitted through covalent cross-links in the entire fibril. On the other hand, ID-onset is related to a stress localization mechanism which is relevant when different molecules within the fibril have significant differences in covalent cross-links occurrence. This likely occurs especially for low cross-link density (thereby, when ID intervenes in fibril mechanics). The ID-related localization mechanism is herein described through the free-energy contribution Ψ_m^{ID} in Eq. (12d), and it is driven by stress σ_c^{ID} in Eq. (29). This modeling choice means that it is herein assumed that ID-onset occurs in correspondence of a molecule where one mature (if $\lambda_c^T \neq 0$) and one immature (if $\lambda_c^D \neq 0$) covalent cross-links are present.

Addressing MR-onset, the free-energy contribution Ψ_m^b in Eq. (16), and thereby molecular stress σ_m (resp., strain ε_m^e) drives this source of damage. In this case, no localization mechanism is modeled because the stress at constituent scale is assumed to be fairly constant within fibrils for high cross-link density (when MR is relevant for fibril mechanics).

The density of mature cross-links is a main factor for the internal damage mechanism which is activated at fibril failure. In case of low mature cross-link density (as in RTT), intermolecular sliding is high (ratio $\varepsilon_c/\varepsilon_m^e$ is closer to the unit with respect to the HPT case in Fig. 8), and thereby, the force transmitted through the covalent cross-links is sufficient for the onset of ID before the one of MR. On the other hand, high density of mature cross-links in HPT is an obstacle for intermolecular sliding with respect to molecular elongation (ε_c remains small compared to ε_m^e in Fig. 8), and thereby, σ_m (resp., ε_m^e) reaches σ_{MR} (resp., ε_{MR}) before that σ_c^{ID} (resp., ε_c) reaches σ_{ID} (resp., ε_{ID}).

Moreover, fibril ultimate stress increases with cross-link density for low cross-link density, and then, it results constant (see Fig. 9). This evidence is related to the transition from ID to MR failure mechanisms, elucidated in the latter figure. Addressing the range of values dominated by ID, when λ_c^T increases, σ_c^{ID} reaches σ_{ID} for higher values of ε_m^e and σ_m (because the higher is the density of mature cross-links, the lower is molecular sway with respect to molecular elongation). Accordingly, since molecular and fibril stress differ only due to the ratio between fibril cross-sectional area $\mathcal{A}_f$ and load-bearing area $\mathcal{A}_c$, fibril strength increases with λ_c^T. On the other hand, addressing the range of values dominated by MR, fibril ultimate stress is constant with λ_c^T and related to molecular ultimate stress, resulting $s_f = \rho_a \sigma_{MR}$. In this case, no further strengthening mechanism is present. Nevertheless, it is worth pointing out that fibril strain at failure, d_f, is much higher than molecular failure strain ε_{MR} because of intermolecular sliding favored by slip-pulse mechanisms (see Fig. 8). Moreover, d_f is fairly constant with λ_c^T with a peak in correspondence of the ID-MR transition.

– *Analysis of modeling choices*

Present work couples the model for intermolecular interactions by Marino and Vairo (2014a) with the one for the nonlinear elasto-damage mechanics of collagen molecules by Maceri et al. (2012b). Accordingly, the sensitivity and the physical meaning of most model parameters have been already discussed in the existing literature and they are here only recalled. Moreover, some refinements for both models have been included starting from the need of fitting experimental data on collagen fibrils. In detail, these are a refined nonlinear activation law for weak cross-links damage (Eq. (11)) and molecular relaxation mechanisms associated with MR (governed by parameter τ_o^{MR}).

The parametric analysis on the values of parameters governing weak cross-links damage highlights the effectiveness of modeling choice. Firstly, it is worth pointing out that from Eq. (11): when $\omega = 0$ and $v_w \to \infty$, then an unlimited damage rate is considered; when $\omega = 0$ and $v_w < +\infty$, then damage rate is limited by the constant v_w. Figure 10 shows that the choice of either an unlimited or a constant damage rate significantly affects the obtained fibril constitutive response but also that, for both choices, SP activation couples with the straightening of the cross-linked telopeptide determining a sharp transition between the decreasing and the increasing branch of E_f. This feature does not agree with experimental data that clearly indicate a smooth variation of E_f. On the other hand, the smoothness of E_f is recovered considering a nonlinear damage activation law governed by Eq. (11) (with $\omega \neq 0$ and $v_w < +\infty$), and it is associated with the convexity of β_2 with ε_f.

Figure 10 shows also that parameter τ_o^{MR} governs fibril brittleness associated with MR. As a general rule of thumb, lower is the value of molecular relaxation decay time constants, higher is the stress decrease rate at failure, and thereby the mechanical response appears more brittle. Thereby, the transition from a yielding softening to a brittle behavior resides only in the difference between the associated molecular relaxation time constants. In this framework, in agreement with MDS data (Buehler 2008; Uzel and Buehler 2011), it is interesting to note that the fitting of experimental data corresponds to values $\tau_o^{ID} > \tau_o^{MR}$, although the typical elongation rates employed for fibril uniaxial traction do not allow to

appreciate significant differences in the stress decay rate at fibril failure (Marino and Vairo 2014a).

• *Reproduction of fibril loading–unloading behavior*

Finally, the model is applied for predicting fibril response to a loading–unloading test (see Fig. 11). The obtained hysteresis loops are fully in agreement with experimental evidence (Shen et al. 2008; Svensson et al. 2010). Thanks to the adopted multiscale rationale, these hysteresis loops are herein related to nanoscale deformation mechanisms and are not described employing phenomenological viscous laws. In fact, the residual strains appearing at the end of each cycle are a straight consequence of the reversibility assumption on intermolecular weak bonds, associated with the activation and deactivation of SP.

• *Model strengths, limitations and future directions*

In summary, accounting for nanoscale mechanisms, the model provides a special insight on the correlation between the histochemical features of collagen fibrils and their mechanics in terms of stiffness, nonlinearities, damage behavior and strength. A quantitative correlation between mature cross-link density and mechanical response is effectively obtained. Elasto-damage molecular and intermolecular mechanisms are explicitly modeled, providing a rational explanation to the nonlinear and viscoelastic mechanics of collagen fibrils.

Despite collagen molecules and fibrils are three-dimensional structures (Orgel et al. 2006; Pradhan et al. 2011), the model is developed within a mono-dimensional framework in order to describe several nanoscale mechanisms in a computational feasible way. Thereby, if coupled with multiscale homogenization methods, present approach allows for an effective upscaling of complex molecular and intermolecular effects in three-dimensional macroscale tissue models. This rationale has been already employed for the description of soft connective tissues (Maceri et al. 2010, 2012a, 2013; Marino and Vairo 2013, 2014b, c), but it is likely suitable also for homogenized models of bones (Hellmich et al. 2004; Grimal et al. 2011; Morin and Hellmich 2013; Morin et al. 2013; Morin and Hellmich 2014).

The model presents some limitations that will be faced in future works. Firstly, the mechanical behavior of non-enzymatic cross-links (namely, advanced glycation end products) is herein not addressed. Moreover, the best fitting of experimental data is obtained when a significant difference in the stiffness of mature (between molecules in different microfibrils/fibrils) and immature (between molecules within the same microfibril) cross-links is considered, resulting $k_c^T / k_c^D \approx 20$. This outcome is likely related to a geometric effect: the assembly of cross-linked microfibrils (helically wounded each other and whose relative sliding is prevented by the presence of intermicrofibrils cross-links) is stiffer than the assembly of non-cross-linked microfibrils (which are free to slide each other due to the absence of intermicrofibrils cross-links). This three-dimensional geometric effect is effectively described in the present mono-dimensional framework by considering a higher stiffness for mature cross-links, but different strategies will be also investigated in future works, by explicitly addressing the microfibril sliding in the formulation of the model.

Furthermore, the model has been validated addressing only traction of fibrils. The analysis of their compressive behavior requires more investigations. Moreover, only two fibrils are employed for comparison between model outcomes and experimental data. Future works will address an higher number of samples. In this framework, a refined automatic procedure for parameter setting will be conceived and implemented. This will allow to obtain physiological ranges for biophysical and biochemical parameters, straightforwardly derived from mechanical measures. Finally, a quantitative correlation between the values of model parameters and more measurable biophysical and biochemical parameters (such as hydration state, pH, ionic environment and enzymatic activity) will be investigated.

In general, thanks to the multiscale rationale herein employed, new or different computational/experimental evidence at nanoscale could be straightforwardly incorporated in present model without affecting its general setting. For instance, interscale compatibility relationships or nanoscale constitutive laws only could be modified in order to obtain refined responses of fibril mechanics.

5 Conclusions

A great modeling challenge in biomechanics is to identify and to upscale molecular and intermolecular mechanisms that are likely to have a significant macroscopic influence. Addressing connective tissues, elasto-damage effects of collagen molecules and their interaction properties within fibrillar structures have to be analyzed across scales up to the continuum level.

In this study, an analytical model of collagen fibril mechanics is developed. The model enriches the model by Marino and Vairo (2014a) that allowed to describe: permanent molecular sliding associated to slip-pulse mechanisms; the delayed activation of the hook-shaped telopeptide in which the covalent cross-links form; interstrand delamination mechanisms associated with the rupture of intramolecular weak bonds. The model has been generalized by taking into account: different responses for mature and immature cross-links; molecular elastic nonlinearities associated with thermal fluctuations, helix uncoiling and stretching of molecular backbone; damage of intramolecular covalent bonds; refined nonlinear slip-pulse activation.

The proposed analytical approach allows to gain a better comprehension on the nanoscale intrafibrillar mechanisms where experimental techniques and atomistic computations reach their limits. Indeed, model effectively predicts how fibril nanostructure affects the nonlinear coupling of the internal mechanisms characterizing fibril mechanics and it allows to run simulations with a very low computational cost. Accordingly, present model might be effectively employed within a structural multiscale approach for developing refined macroscale models of biological tissues (Maceri et al. 2010, 2012a, 2013; Marino and Vairo 2013, 2014b, c). Thereby, it represents a powerful tool for investigating on the structure mechanics dependence in biological tissues. This opens toward the analysis of histochemical alterations associated with pathological tissue/organ behavior, as well as the investigation on the effectiveness of pharmacological treatments favoring the homeostatic histochemical condition.

Acknowledgments The author gratefully acknowledges Prof. Peter Wriggers, Prof. Franco Maceri and Prof. Giuseppe Vairo for fruitful discussions on the topics addressed by present paper. Present study was supported by the Italian Minister of University and Research MIUR (PRIN, Grant Number F11J12000210001) and by a research fellowship for postdoctoral researchers of the Alexander von Humboldt Foundation.

Appendix: Basics of convex analysis

In agreement with classical arguments of convex analysis, introduce the set $\bar{\mathbb{R}} = \mathbb{R} \cup \{+\infty\}$ where the regular addition is completed by the rules: $a + (+\infty) = +\infty$ $(\forall\, a \in \mathbb{R})$ and $+\infty + (+\infty) = +\infty$, while multiplication by strictly positive numbers is completed by $a \times (+\infty) = +\infty$ $(\forall\, a \in \mathbb{R}^+)$, (Frémond 2002). In this framework, introduce the indicator functions

$$\mathrm{I}_{[a,b]} : \mathbb{R} \mapsto \bar{\mathbb{R}}, \quad \mathrm{I}_{[a,b]}(x) = \begin{cases} 0 & \text{if } x \in [a,b] \\ +\infty & \text{else} \end{cases},$$

$$\mathrm{I}^+ : \mathbb{R} \mapsto \bar{\mathbb{R}}, \quad \mathrm{I}^+(x) = \begin{cases} 0 & \text{if} x \geq 0 \\ +\infty & \text{else} \end{cases},$$

with their subdifferential sets being

$$\partial \mathrm{I}_{[a,b]}(x) = \begin{cases} p \leq 0 & \text{if } x = a \\ 0 & \text{if } a < x < b \\ p \geq 0 & \text{if } x = b \\ \nexists & \text{else} \end{cases},$$

$$\partial \mathrm{I}^+(x) = \begin{cases} p \leq 0 & \text{if } x = 0 \\ 0 & \text{if } x > 0 \\ \nexists & \text{if } x < 0 \end{cases}.$$

References

Andreassen T, Seyer-Hansen K, Bailey A (1981) Thermal stability, mechanical properties and reducible cross-links of rat tail tendon in experimental diabetes. Biochim Biophys Acta Gen Subj 677:313–317

Avery NC, Bailey AJ (2008) Restraining cross-links responsible for the mechanical properties of collagen fibers: natural and artificial. In: Fratzl P (ed) Collagen: structure and mechanics. Springer, Berlin, pp 81–110

Bailey AJ, Paul RG, Knott L (1998) Mechanisms of maturation and ageing of collagen. Mech Ageing Dev 106:1–56

Bailey AJ (2001) Molecular mechanisms of ageing in connective tissues. Mech Ageing Dev 122:735–755

Bozec L, Horton M (2005) Topography and mechanical properties of single molecules of type I collagen using atomic force microscopy. Biophys J 88:4223–4231

Brüel A, Ørtoft G, Oxlund H (1998) Inhibition of cross-links in collagen is associated with reduced stiffness of the aorta in young rats. Atherosclerosis 140:135–145

Buehler MJ (2006) Atomistic and continuum modeling of mechanical properties of collagen: elasticity, fracture, and self-assembly. J Mater Res 21:1947–1961

Buehler MJ (2008) Nanomechanics of collagen fibrils under varying cross-link densities: atomistic and continuum studies. J Mech Behav Biomed Mater 1:59–67

Buehler MJ, Wong SY (2007) Entropic elasticity controls nanomechanics of single tropocollagen molecules. Biophys J 93:37–43

Carmo M, Colombo L, Bruno A, Corsi FRM, Roncoroni L, Cuttin MS, Radice F, Mussini E, Settembrini PG (2002) Alteration of elastin, collagen and their cross-links in abdominal aortic aneurysms. Eur J Vasc Endovasc Surg 23:543–549

Cusack S, Miller A (1979) Determination of the elastic constants of collagen by Brillouin light scattering. J Mol Biol 135:39–51

DeGroot J, Verzijl N, Wenting-Van Wijk MJG, Jacobs KMG, Van El B, Van Roermund PM, Bank RA, Bijlsma JWJ, TeKoppele JM, Lafeber FPJG (2004) Accumulation of advanced glycation end products as a molecular mechanism for aging as a risk factor in osteoarthritis. Arthritis Rheum 50:1207–1215

Depalle B, Qin Z, Shefelbine SJ, Buehler MJ (2014) Influence of cross-link structure, density and mechanical properties in the mesoscale deformation mechanisms of collagen fibrils. J Mech Behav Biomed Mater. doi:10.1016/j.jmbbm.2014.07.008

Eyre DR, Wu JJ (2005) Collagen cross-links. In: Brinckmann J, Notbohm H, Müller PK (ed) Collagen: primer in structure, processing and assembly. Topics in current chemistry, vol 247. Springer, Berlin, pp 207–229

Eyre DR, Koob TJ, Van Ness KP (1984) Quantitation of hydroxypyridinium crosslinks in collagen by high-performance liquid chromatography. Anal Biochem 137:380–388

Eyre DR, Weis MA, Wu JJ (2008) Advances in collagen cross-link analysis. Methods 45:65–74

Fessel G, Gerber C, Snedeker JG (2012) Potential of collagen cross-linking therapies to mediate tendon mechanical properties. J Shoulder Elbow Surg 21:209–217

Fratzl P (2008) Collagen: structure and mechanics. Springer, Berlin

Frémond M (2002) Non-smooth thermomechanics. Springer, Berlin

Gautieri A, Pate MI, Vesentini S, Redaelli A, Buehler MJ (2012) Hydration and distance dependence of intermolecular shearing between collagen molecules in a model microfibril. J Biomech 45:2079–2083

Gautieri A, Redaelli A, Buehler MJ, Vesentini S (2014) Age-and diabetes-related non enzymatic cross links in collagen fibrils: candidate amino acids involved in Advanced Glycation End-products. Matrix Biol 34:89–95

Germain P, Nguyen QS, Suquet P (1983) Continuum thermodynamics. J Appl Mech 50:1010–1020
Grant CA, Brockwell DJ, Radford SE, Thomson NH (2009) Tuning the elastic modulus of hydrated collagen fibrils. Biophys J 97:2985–2992
Grimal Q, Rus G, Parnell WJ, Laugier P (2011) A two-parameter model of the effective elastic tensor for cortical bone. J Biomech 44:1621–1625
Hain M, Wriggers P (2008) Numerical homogenization of hardened cement paste. Comput Mech 42:197–212
Hellmich C, Barthélémy JF, Dormieux L (2004) Mineral-collagen interactions in elasticity of bone ultrastructure–a continuum micromechanics approach. Eur J Mech A Solids 23:783–810
Holmes DF, Graham HK, Trotter JA, Kadler KE (2001) STEM/TEM studies of collagen fibril assembly. Micron 32:273–285
Holzapfel GA, Ogden RW (2010) On the bending and stretching elasticity of biopolymer filaments. J Elast 104:319–342
Klepeis JL, Lindorff-Larsen K, Dror RO, Shaw DE (2009) Long-timescale molecular dynamics simulations of protein structure and function. Curr Opin Chem Biol 19:120–127
Kouznetsova V, Brekelmans WAM, Baaijens FPT (2001) An approach to micro-macro modeling of heterogenous materials. Comput Mech 27:37–48
Lehmann E, Loehnert S, Wriggers P (2012) Computational homogenization of polycrystalline elastoplastic microstructures at finite deformation. Tech Mech 37:369–379
Li Y, Fessel G, Georgiadis M, Snedker JG (2013) Advanced glycation end-products diminish tendon collagen fiber sliding. Matrix Biol 32:169–177
Maceri F, Marino M, Vairo G (2010) A unified multiscale mechanical model for soft collagenous tissues with regular fiber arrangement. J Biomech 43:355–363
Maceri F, Marino M, Vairo G (2012a) An insight on multiscale tendon modeling in muscle-tendon integrated behavior. Biomech Model Mechanobiol 11:505–517
Maceri F, Marino M, Vairo G (2012b) Elasto-damage modeling of biopolymer molecules response. CMES 87:461–481
Maceri F, Marino M, Vairo G (2013) Age-dependent arterial mechanics via a multiscale elastic approach. Int J Comput Methods Eng Sci Mech 14:141–151
Marino M (2013) Pseudopotentials and thermomechanical response of materials and structures: a convex analysis approach. Dissertation, Department of Civil Engineering and Computer Science, University of Rome "Tor Vergata"
Marino M, Vairo G (2013) Multiscale elastic models of collagen biostructures: from cross-linked molecules to soft tissues. In: Gefen A (ed) Computational modelling of biomechanics and biotribology in the musculoskeletal system. Stud. Mechanobiol. Tissue Eng Biomater, vol 14. Springer, Berlin, pp 73–102
Marino M, Vairo G (2014a) Influence of inter-molecular interactions on the elasto-damage mechanics of collagen fibrils: a bottom-up approach towards macroscopic tissue modeling. J Mech Phys Solids 73:38–54
Marino M, Vairo G (2014b) Stress and strain localization in stretched collagenous tissues via a multiscale modelling approach. Comput Methods Biomech Biomed Eng 17:11–30
Marino M, Vairo G (2014c) Computational modeling of soft tissues and ligaments. In: Jin Z (ed) Computational modelling of biomechanics and biotribology in the musculoskeletal system. Woodhead Publ Ser Biomat, vol 81. Woodhead Publishing Limited, Cambridge, pp 141–172
Marko JF, Siggia ED (1995) Stretching DNA. Macromolecules 28:8759–8770
Miles CA, Bailey AJ (2001) Thermally labile domains in the collagen molecule. Micron 32:325–332
Misof K, Rapp G, Fratzl P (1997) A new molecular model for collagen elasticity based on synchrotron X-ray scattering evidence. Biophys J 72:1376–1381
Morin C, Hellmich C, Henits P (2013) Fibrillar structure and elasticity of hydrating collagen: a quantitative multiscale approach. J Theor Biol 317:384–393
Morin C, Hellmich C (2013) Mineralization-driven bone tissue evolution follows from fluid-to-solid phase transformations in closed thermodynamic systems. J Theor Biol 335:185–197
Morin C, Hellmich C (2014) A multiscale poromicromechanical approach to wave propagation and attenuation in bone. Ultrasonics 54:1251–1269
Orgel J, Wess TJ, Miller A (2000) The in situ conformation and axial location of the intermolecular cross-linked non-helical telopeptides of type I collagen. Structure 8:137–142
Orgel JPRPO, Irving TC, Miller A, Wess T (2006) Microfibrillar structure of type I collagen in situ. Proc Nat Acad Sci USA 103:9001–9005
Pradhan SM, Katti DR, Katti KS (2011) Steered molecular dynamics study of mechanical response of full length and short collagen molecules. J Nanomech Micromech 1:104–110
Reiser K, McCormick RJ, Rucker RB (1996) Enzymatic and nonenzymatic cross-linking of collagen and elastin. FASEB J 6:2439–2449
Saito M, Marumo K, Fujii K, Ishioka N (1997) Single-column high-performance liquid chromatographic-fluorescence detection of immature, mature, and senescent cross-links of collagen. Anal Biochem 253:26–32
Sasaki N, Odajima S (1996) Elongation mechanism of collagen fibrils and force-strain relations of tendon at each level of structural hierarchy. J Biomech 29:1131–1136
Shen ZL, Dodge MR, Kahn H, Ballarini R, Eppell SJ (2008) Stress-strain experiments on individual collagen fibrils. Biophys J 95:3956–3963
Svensson RB, Hassenkam T, Hansen P, Magnusson SP (2010) Viscoelastic behavior of discrete human collagen fibrils. J Mech Behav Biomed Mater 3:112–115
Svensson RB, Mulder H, Kovanen V, Magnusson SP (2013) Fracture mechanics of collagen fibrils: influence of natural cross-links. Biophys J 104:2476–2484
Uzel S, Buehler MJ (2011) Molecular structure, mechanical behavior and failure mechanism of the C-terminal cross-link domain in type I collagen. J Mech Behav Biomed Mater 4:153–161
Verzijl N, DeGroot J, Ben ZC, Brau-Benjamin O, Maroudas A, Bank RA, Mizrahi J, Schalkwijk CG, Thorpe SR, Baynes JW, Bijlsma JWJ, Lafeber FPJG, TeKoppele JM (2002) Crosslinking by advanced glycation end products increases the stiffness of the collagen network in human articular cartilage: a possible mechanism through which age is a risk factor for osteoarthritis. Arthritis Rheum 46:114–123
Wess TJ (2008) Collagen fibrillar structure and hierarchies. In: Fratzl P (ed) Collagen: structure and mechanics. Springer, Berlin, pp 49–80
Yang L, van der Werf KO, Dijkstra PJ, Feijen J, Bennink ML (2012) Micromechanical analysis of native and cross-linked collagen type I fibrils supports the existence of microfibrils. J Mech Behav Biomed Mater 6:148–158
Zimmermann E, Schaible E, Bale H, Barth HD, Tang SY, Reichert P, Busse B, Alliston T, Ager JW III, Ritchie RO (2011) Age-related changes in the plasticity and toughness of human cortical bone at multiple length scales. Proc Nat Acad Sci USA 108:14416–14421